were determined by the trypan blue exclusion method. The cells were suspended in 0.5 ml saline and the radioactivity assayed as described above.

Uptake by HepG2 Cells

The HepG2 cells were plated on a 12-well cluster dish at a density of 2×10^5 cells/3.8 cm^2 and cultivated in 800 μl DMEM supplemented with 10% FBS. Twenty-four hours later, the culture medium was replaced with an equivalent volume of HBSS containing [^{3}H]liposomes (0.25 mg/ml, 1.8 kBq/ml). For the inhibition study, 20 mM galactose was added to the liposome solution. After incubation for 1 h at 37°C, the solution was removed by aspiration, and the cells were washed five times with ice-cold HBSS buffer. For separation of the internalized and surface bound liposomes, the cells were washed three times with acetate buffer (pH 4) to remove the liposomes bound to the cell surface. The cells were then solubilized in 0.5 ml 1 M NaOH and the radioactivity was assayed as above. The protein content of each sample was determined by a modification of the Lowry method. In another set of experiments, the cells were pre-incubated with HBSS containing 10 mM NaN_3 for 20 min prior to the addition of liposomes.

Statistical Analysis

Differences were statistically evaluated by one-way analysis of variance followed by the Student-Newmann–Keuls multiple comparison test. The level of significance was set at $p < 0.05$.

RESULTS

Liposome Size

Table I summarizes the lipid composition and particle size of the liposomes prepared. All liposomes were similar in size (average diameter approximately 90 nm). The size of the liposomes remained constant over one month at 4°C.

Tissue Disposition of Liposomes after Intravenous Injection

Figure 1 shows the tissue disposition of [^{3}H]DSPC/Chol (60:40), [^{3}H]DSPC/Chol/Gal-C4-Chol (60:35:5), [^{3}H]DSPC/Chol (90:10), and [^{3}H]DSPC/Chol/Gal-C4-Chol (90:5:5) liposomes in mice. When intravenously injected, [^{3}H]DSPC/Chol/Gal-C4-Chol (60:35:5) and [^{3}H]DSPC/Chol/Gal-C4-Chol (90:5:5) were rapidly taken up by the liver (Fig.1), as well as other galactosylated liposomes (data not shown). On the other hand, [^{3}H]DSPC/Chol (60:40) liposomes exhibited prolonged retention in the blood circulation (Fig. 1A). However, [^{3}H]DSPC/Chol (90:10) liposomes were taken up by the liver almost as fast as their galactosylated counterpart (Fig. 1C and D).

Table I. Lipid Composition and Particle Size of Liposomes

Liposome (molar ratio)	Particle size (mm)[a]
DSPC/Chol (50:50)	88.7 ± 10.5
DSPC/Chol (60:40)	94.6 ± 6.3
DSPC/Chol (70:30)	89.4 ± 6.7
DSPC/Chol (90:10)	91.7 ± 12.8
DSPC/Chol/Gal-C4-Chol (50:45:5)	94.7 ± 7.9
DSPC/Chol/Gal-C4-Chol (60:35:5)	84.0 ± 14.8
DSPC/Chol/Gal-C4-Chol (70:25:5)	93.9 ± 9.7
DSPC/Chol/Gal-C4-Chol (90:5:5)	85.8 ± 10.8

[a] The particle size of the liposomes was measured using a dynamic light scattering spectrophotometer. Results are expressed as the mean ± SD of three determinations.

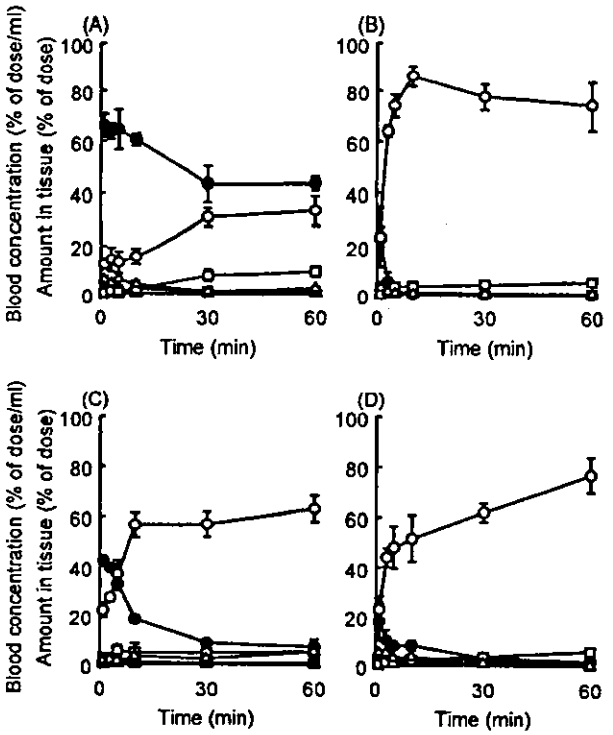

Fig. 1. Time-courses of the concentration in blood and amounts in tissues of ^{3}H-radioactivity after intravenous injection of (A) [^{3}H]DSPC/Chol (60:40), (B) [^{3}H]DSPC/Chol/Gal-C4-Chol (60:35:5), (C) [^{3}H]DSPC/Chol (90:10) and (D) [^{3}H]DSPC/Chol/Gal-C4-Chol (90:5:5) liposomes into mice at a dose of 25 mg/kg. Results are expressed as the mean ± SD of three mice. Keys: (●) blood; (○) liver; (■) kidney; (□) spleen; (▲) heart; (△) lung.

Pharmacokinetic Analysis of Liposomes

Figure 2 summarizes the liver uptake clearance (CL_{liver}) of all the liposomes investigated after intravenous injection into mice. The CL_{liver} of liposomes lacking galactose units was much lower than that of galactosylated liposomes. Among the control liposomes ([^{3}H]DSPC/Chol liposomes), the DSPC/Chol (90:10) liposomes with the smallest Chol ratio had the highest CL_{liver}.

The CL_{liver} of [^{3}H]DSPC/Chol/Gal-C4-Chol (50:45:5), [^{3}H]DSPC/Chol/Gal-C4-Chol (60:35:5), and [^{3}H]DSPC/Chol/Gal-C4-Chol (70:25:5) liposomes was, respectively, 51.4, 52.2, and 48.8-times greater than that of the counterparts without Gal-C4-Chol, whereas that of [^{3}H]DSPC/Chol/Gal-C4-Chol (90:5:5) liposomes was only 2.9-times greater than that of [^{3}H]DSPC/Chol (90:10) liposomes. Although all the galactosylated liposomes tested were equivalent in terms of the number of galactose units per liposome, [^{3}H]DSPC/Chol/Gal-C4-Chol (60:35:5) liposomes had the highest CL_{liver}.

Cellular Localization of Liposomes in the Liver

Figure 3 shows the distribution of [^{3}H]DSPC/Chol (60:40), [^{3}H]DSPC/Chol/Gal-C4-Chol (60:35:5), [^{3}H]DSPC/Chol

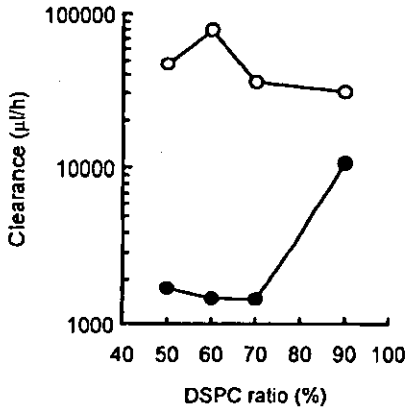

Fig. 2. Hepatic clearance (CL_{liver}) of liposomes after intravenous injection in mice at a dose of 25 mg/kg. The CL_{liver} was calculated by dividing the amount in the liver at 10 min by the area under the blood concentration-time curve up to the same time as described in Materials and Methods. The CL_{liver} values were plotted against the percentage of DSPC in liposome total lipids. Keys: (●) liposomes without Gal-C4-Chol; (○) liposomes with Gal-C4-Chol.

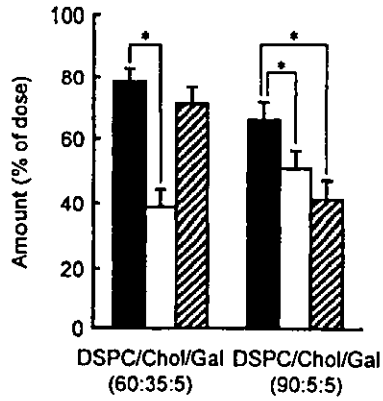

Fig. 4. Amount of ^{3}H-radioactivity in the liver after intravenous injection of [^{3}H]liposomes with or without preinjection of 20mg/kg Gal-BSA or 250mg/kg DSPC/Chol (90:10) liposomes. The distribution was examined at 5 min after intravenous injection of [^{3}H]liposomes. Results are expressed as the mean ± SD of three mice. Keys: (filled) no preinjection; (open) preinjection of Gal-BSA; (hatched) preinjection of DSPC/Chol liposomes. * Statistically significant differences ($p < 0.05$) from each no preinjection group.

(90:10), and [^{3}H]DSPC/Chol/Gal-C4-Chol (90:5:5) liposomes between hepatocytes and NPC at 30 min after intravenous injection. [^{3}H]DSPC/Chol/Gal-C4-Chol (60:35:5) liposomes were taken up preferentially by hepatocytes compared with NPC (hepatocytes/NPC ratio of 15), whereas [^{3}H]DSPC/Chol (60:40) liposomes were taken up to an equal extent by both hepatocytes and NPC. On the other hand, NPC uptake was marked in the case of [^{3}H]DSPC/Chol (90:10) liposomes. [^{3}H]DSPC/Chol/Gal-C4-Chol (90:5:5) liposomes exhibited greater distribution to hepatocytes compared with [^{3}H]DSPC/Chol (90:10) liposomes, but the uptake by hepatocytes did not exceed that in NPC. The hepatocyte/NPC ratio was calculated to be 0.78, which was much smaller than that for [^{3}H]DSPC/Chol/Gal-C4-Chol (60:35:5) liposomes.

Effect of Gal-BSA or DSPC/Chol (90:10) Liposomes on Hepatic Uptake of Galactosylated Liposomes

Figure 4 shows the effect of preinjection of a large amount of Gal-BSA or DSPC/Chol (90:10) liposomes on the hepatic uptake of [^{3}H]DSPC/Chol/Gal-C4-Chol (60:35:5) and [^{3}H]DSPC/Chol/Gal-C4-Chol (90:5:5) liposomes. Gal-BSA significantly inhibited the hepatic uptake of both [^{3}H]DSPC/Chol/Gal-C4-Chol (60:35:5) and [^{3}H]DSPC/Chol/Gal-C4-Chol (90:5:5) liposomes. The extent of the inhibition by Gal-BSA, however, was greater for [^{3}H]DSPC/Chol/Gal-C4-Chol (60:35:5) liposomes than for [^{3}H]DSPC/Chol/Gal-C4-Chol (90:5:5) liposomes.

Preinjection of DSPC/Chol (90:10) liposomes had no significant effects on the hepatic uptake of [^{3}H]DSPC/Chol/Gal-C4-Chol (60:35:5) liposomes whereas the injection of DSPC/Chol (90:10) liposome prior to [^{3}H]DSPC/Chol/Gal-C4-Chol (90:5:5) liposomes significantly inhibited the hepatic uptake of the latter.

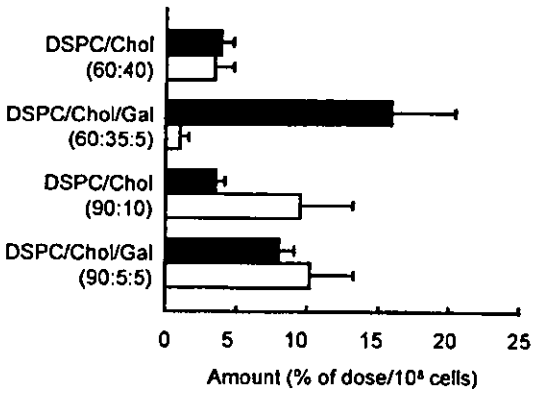

Fig. 3. Distribution of ^{3}H-radioactivity between hepatocytes and liver NPC at 30 min after intravenous injection of [^{3}H]liposomes into mice at a dose of 25 mg/kg. Results are expressed as the mean ± SD of three mice. Key: (filled) hepatocytes; (open) NPC.

Uptake by HepG2 Cells

Figure 5 shows the *in vitro* uptake of [^{3}H]liposomes in HepG2 cells. The uptake of [^{3}H]DSPC/Chol/Gal-C4-Chol (60:35:5) and [^{3}H]DSPC/Chol/Gal-C4-Chol (90:5:5) lipo-

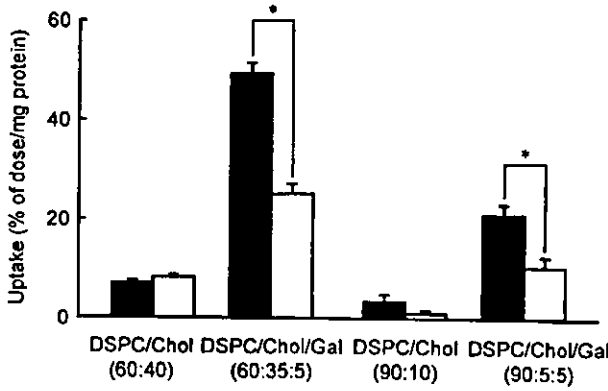

Fig. 5. Uptake of [^{3}H]liposomes by HepG2 cells. Cells were incubated with each type of [^{3}H]liposome with or without 20 mM galactose. The amount of ^{3}H-radioactivity associated with the cells was measured following 1 h of incubation. Results are expressed as the mean ± SD of three wells. Keys: (filled) control; (open) +20 mM galactose. * Statistically significant differences ($p < 0.05$).

somes was greater than that of [^{3}H]DSPC/Chol (60:40) and [^{3}H]DSPC/Chol (90:10) liposomes, respectively. The uptake of the galactosylated liposomes was significantly inhibited by the addition of 20mM galactose, whereas no change was observed with control liposomes. [^{3}H]DSPC/Chol/Gal-C4-Chol (60:35:5) liposomes showed significantly higher uptake than [^{3}H]DSPC/Chol/Gal-C4-Chol (90:5:5) liposomes.

The amount of surface binding and internalization of the galactosylated liposomes was evaluated according to an acid-wash procedure (Fig. 6). The surface binding of both [^{3}H]DSPC/Chol/Gal-C4-Chol (60:35:5) and [^{3}H]DSPC/Chol/Gal-C4-Chol (90:5:5) liposomes was similar although the amount of [^{3}H]DSPC/Chol/Gal-C4-Chol (60:35:5) liposomes internalized was greater than that of [^{3}H]DSPC/Chol/Gal-C4-Chol (90:5:5) liposomes. When the cells were treated with a metabolic inhibitor, NaN_3, the amount associated with the cells was similar in both galactosylated liposomes, and comparable with the acid-washable amounts under normal conditions.

DISCUSSION

Asialoglycoprotein receptor-mediated targeting of pharmaceuticals to hepatocytes is a promising approach to achieve cell (hepatocyte)-specific delivery after systemic administration because (i) the asialoglycoprotein receptors are specifically expressed in hepatocytes, (ii) molecules entering the systemic circulation easily get access to the cells through the discontinuous endothelium of the liver, and (iii) the liver has a high blood flow. These physiologic and biologic features of the liver and hepatocytes give galactosylated carriers the opportunity to deliver drugs to hepatocytes via asialoglycoprotein receptor-mediated endocytosis.

As far as the interaction of a galactosylated ligand with the receptors is concerned, the affinity of the ligand seems to be governed by the valency of the galactose residues and their

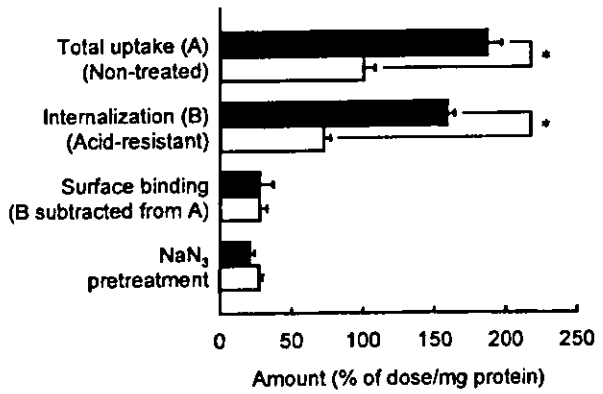

Fig. 6. Amount of [^{3}H]galactosylated liposomes associated with HepG2 cells. Cells were incubated with [^{3}H]DSPC/Chol/Gal-C4-Chol (60:35:5) or [^{3}H]DSPC/Chol/Gal-C4-Chol (90:5:5) liposomes. At 1 h, the cells were washed with an acid buffer to separate the surface bound liposomes. The difference in cellular association between acid-treatment and no treatment was regarded as the amount associated with the cell surface. In another group, the cells were pre-incubated with HBSS containing 10 mM NaN_3 for 20 min prior to the addition of liposomes. Results are expressed as the mean ± SD of three wells. Keys: (filled) [^{3}H]DSPC/Chol/Gal-C4-Chol (60:35:5) liposome; (open) [^{3}H]DSPC/Chol/Gal-C4-Chol (90:5:5) liposome. * Statistically significant differences ($p < 0.05$).

appropriate spacing. Clustering of galactosides greatly enhances the affinity for the receptor in the following order: tetra- > tri- >> bi- >> mono-antennary galactosides (17). Such an effect can be explained by the simultaneous occupation of the carbohydrate recognition domains of the receptor and optimal structures of cluster galactosides for binding have been proposed (18). Based on these findings, various oligosaccharides containing multiple galactose terminals have been developed as "homing" devices with a high affinity for hepatocytes (19–21). These synthetic oligosaccharide-containing molecules as well as naturally occurring asialoglycoproteins are believed to have a high affinity for asialoglycoprotein receptors.

In previous papers, we have described the modification of various macromolecules with IME-thiogalactoside to obtain galactosylated derivatives. The pharmacokinetic study of galactosylated macromolecules in mice revealed that a derivative having a sufficient number of galactose units is very efficiently recognized by the receptors *in vivo* and is taken up by the liver at a rate equal to the hepatic plasma flow (3–5). These results indicate that, although monosaccharides such as IME-thiogalactoside have a much weaker receptor affinity than oligosaccharides, the clustering of monosaccharides on a carrier can compensate for this weak affinity. The estimated density of galactose units on the protein surface was found to determine the affinity of galactosylated proteins for the asialoglycoprotein receptors *in vivo* (4). Based on these findings, we have designed a series of mono-glycosylated derivatives of cholesterol to obtain glycosylated lipophilic carriers such as liposomes and lipid emulsions (7,22,23). Galactosylated liposomes consisting of Gal-C4-Chol and other lipids have been shown to be promising carriers for the delivery of drugs or genes to asialoglycoprotein receptor-positive cells (7–11,22,23).

As clearly shown with galactosylated proteins (4), extensive modification of liposomes with Gal-C4-Chol, for example, 5 mol % of total lipid, can give them the ability to target hepatocytes (9,10). In the present study, both galactosylated liposomes, i.e., [^{3}H]DSPC/Chol/Gal-C4-Chol (60:35:5) and [^{3}H]DSPC/Chol/Gal-C4-Chol (90:5:5) liposomes, exhibited marked accumulation in the liver following intravenous injection in mice. However, the uptake of [^{3}H]DSPC/Chol/Gal-C4-Chol (90:5:5) liposomes was not selective for hepatocytes, whereas that of [^{3}H]DSPC/Chol/Gal-C4-Chol (60:35:5) liposomes was highly selective for these cells. The introduction of a galactose moiety onto a liposome might not necessarily be a universal approach to endow the liposome with the ability to target hepatocytes, because the tissue disposition of galactosylated liposomes is determined not only by the recognition by asialoglycoprotein receptors, but by the other interactions within the body after systemic administration. Low-Chol liposomes are known to have a very short half-life in the circulation, largely due to their extensive uptake by MPS. On the other hand, high-Chol liposomes (30–50 mol % of total lipid) are relatively stable in the circulation (14). Semple *et al.* (13) found that cholesterol-free DSPC liposomes bind significant amounts of serum proteins, whereas cholesterol-rich DSPC liposomes are much less active. These characteristics of low-Chol DSPC liposomes would explain the uptake of [^{3}H]DSPC/Chol/Gal-C4-Chol (90:5:5) liposomes by liver NPC (Fig. 3). Inhibition studies clearly showed that the hepatic uptake of [^{3}H]DSPC/Chol/Gal-C4-Chol (90:5:5) liposomes takes place by at least two different pathways:

galactose-specific hepatocyte uptake and DSPC/Chol (90:10) liposome-sensitive NPC uptake.

The uptake experiments using HepG2 cells *in vitro* were performed to gain further insights into the receptor-mediated uptake of the two different galactosylated liposomes. Compared with galactose-free control liposomes, both [^{3}H]DSPC/Chol/Gal-C4-Chol (60:35:5) and [^{3}H]DSPC/Chol/Gal-C4-Chol (90:5:5) liposomes showed greater and galactose-inhibitable cellular uptake. However, the uptake by HepG2 cells was greater for [^{3}H]DSPC/Chol/Gal-C4-Chol (60:35:5) liposomes than for [^{3}H]DSPC/Chol/Gal-C4-Chol (90:5:5) liposomes. The separation of surface-bound liposomes from their internalized counterparts by acid washing shows that the difference in their uptake can be fully explained by the amount internalized. In a previous paper (25), we analyzed the hepatic uptake of Gal-BSAs with varying numbers of galactose units in isolated, perfused rat liver, and found that the internalization rate of Gal-BSA was greater for derivatives with many galactose residues (i.e., 17 or 36 galactose units/BSA) than for one with only 10 residues. In this case, however, it should be noted that the two galactosylated liposomes investigated contain the same concentration of galactose units. A possible explanation for this is that distribution of Gal-C4-Chol in bilayers may be heterogeneous so that it can affect the rate of internalization via asialoglycoprotein receptor-mediated endocytosis. At lower Chol concentrations, a lateral-phase separation occurs in DSPC/Chol liposomes, (i.e., a pure phospholipid (PC) phase and a PC/Chol mixture phase), whereas high-Chol liposomes possesses a homogeneous, liquid ordered structure (26,27). Such a structural difference depending on the Chol concentration would affect the distribution and mobility of Gal-C4-Chol in bilayers. It has also been reported that membrane lipids are rearranged in bilayers following an interaction with plasma proteins (28), ganglioside-containing liposomes (29), and a polycation (30). This would depend on the rate of lateral diffusion in liposomal bilayers. Overall, slower accumulation of [^{3}H]DSPC/Chol/Gal-C4-Chol (90:5:5) liposomes in the liver compared with Chol-rich galactosylated liposomes (Fig. 1) could also be explained by inappropriate distribution of galactose units on the liposomal surface, although a partial shielding of galactose units by serum protein binding cannot be ruled out.

In conclusion, the lipid composition of galactosylated liposomes has been shown to be important for their targeted delivery to hepatocytes. Besides non-specific serum protein binding, the rate of internalization via a specialized uptake process is affected. The Chol-rich galactosylated liposomes appear to be promising carriers that can expand the specificity of their delivery to the target.

ACKNOWLEDGMENTS

This study is supported in part by a Grant-in-Aid for Scientific Research from the Ministry of Education, Culture, Sports, Science, and Technology of Japan.

REFERENCES

1. G. Ashwell and J. Harford. Carbohydrate-specific receptors of the liver. *Annu. Rev. Biochem.* 51:531–554 (1982).
2. Y. C. Lee, R. R. Townsend, M. R. Hardy, J. Lönngren, J. Arnarp, M. Haraldsson, and H. Lönn. Binding of synthetic oligosaccharides to the hepatic Gal/GalNAc lectin. Dependence on fine structural features. *J. Biol. Chem.* 258:199–202 (1983).
3. M. Nishikawa, H. Hirabayashi, Y. Takakura, and M. Hashida. Design for cell-specific targeting of proteins utilizing sugar-recognition mechanism: effect of molecular weight of proteins on targeting efficiency. *Pharm. Res.* 12:209–214 (1995).
4. M. Nishikawa, C. Miyazaki, F. Yamashita, Y. Takakura, and M. Hashida. Galactosylated proteins are recognized by the liver according to the surface density of galactose moieties. *Am. J. Physiol.* 268:G849–G856 (1995).
5. H. Hirabayashi, M. Nishikawa, Y. Takakura, and M. Hashida. Development and pharmacokinetics of galactosylated poly-L-glutamic acid as a biodegradable carrier for liver-specific drug delivery. *Pharm. Res.* 13:880–884 (1996).
6. T. M. Allen. Long-circulating (sterically stabilized) liposomes for targeted drug delivery. *Trends Pharmacol. Sci.* 15:215–220 (1994).
7. S. Kawakami, F. Yamashita, M. Nishikawa, Y. Takakura, and M. Hashida. Asialoglycoprotein receptor-mediated gene transfer using novel galactosylated cationic liposomes. *Biochem. Biophys. Res. Commun.* 252:78–83 (1998).
8. S. Kawakami, S. Fumoto, M. Nishikawa, F. Yamashita, and M. Hashida. In vivo gene delivery to the liver using novel galactosylated cationic liposomes. *Pharm. Res.* 17:306–313 (2000).
9. S. Kawakami, C. Munakata, S. Fumoto, F. Yamashita, and M. Hashida. Targeted delivery of prostaglandin E_1 to hepatocytes using galactosylated liposomes. *J. Drug Target.* 8:137–142 (2000).
10. Y. Hattori, S. Kawakami, F. Yamashita, and M. Hashida. Controlled biodistribution of galactosylated liposomes and incorporated probucol in hepatocyte-selective drug targeting. *J. Control. Release* 69:369–377 (2000).
11. S. Kawakami, C. Munakata, S. Fumoto, F. Yamashita, and M. Hashida. Novel galactosylated liposomes for hepatocyte-selective targeting of lipophilic drugs. *J. Pharm. Sci.* 90:105–113 (2001).
12. A. Chonn, S. C. Semple, and P. R. Cullis. Association of blood proteins with large unilamellar liposomes in vivo. Relation to circulation lifetimes. *J. Biol. Chem.* 267:18759–18765 (1992).
13. S. C. Semple, A. Chonn, and P. R. Cullis. Influence of cholesterol on the association of plasma proteins with liposomes. *Biochemistry* 35:2521–2525 (1996).
14. J. H. Senior. Fate and behavior of liposomes in vivo: a review of controlling factors. *Crit. Rev. Ther. Drug Carrier Syst.* 3:123–193 (1987).
15. T. Takino, C. Nakajima, Y. Takakura, H. Sezaki, and M. Hashida. Controlled biodistribution of highly lipophilic drugs with various parenteral formulations. *J. Drug Target.* 1:117–124 (1993).
16. A. G. Morell, R. A. Irvine, I. Sternlieb, I. H. Scheinberg, and G. Ashwell. Physical and chemical studies on ceruloplasmin. V. Metabolic studies on sialic acid-free ceruloplasmin in vivo. *J. Biol. Chem.* 243:155–159 (1968).
17. D. T. Connolly, R. R. Townsend, K. Kawaguchi, W. R. Bell, and Y. C. Lee. Binding and endocytosis of cluster glycosides by rabbit hepatocytes. Evidence for a short-circuit pathway that does not lead to degradation. *J. Biol. Chem.* 257:939–945 (1982).
18. Y. C. Lee, R. R. Townsend, M. R. Hardy, J. Lonngren, J. Arnarp, M. Haraldsson, and H. Lonn. Binding of synthetic oligosaccharides to the hepatic Gal/GalNAc lectin. Dependence on fine structural features. *J. Biol. Chem.* 258:199–202 (1983).
19. R. T. Lee, P. Lin, and Y. C. Lee. New synthetic cluster ligands for galactose/N-acetylgalactosamine-specific lectin of mammalian liver. *Biochemistry* 23:4255–4261 (1984).
20. H. H. Spanjer, T. J. C. van Berkel, G. L. Scherphof, and H. J. M. Kempen. The effect of a water-soluble tris-galactoside terminated cholesterol derivative on the in vivo fate of small unilamellar vesicles in rats. *Biochim. Biophys. Acta* 816:396–402 (1985).
21. E. A. Biessen, D. M. Beuting, H. C. Roelen, G. A. van de Marel, J. H. van Boom, and T. J. C. van Berkel. Synthesis of cluster galactosides with high affinity for the hepatic asialoglycoprotein receptor. *J. Med. Chem.* 38:1538–1546 (1995).
22. S. Kawakami, A. Sato, M. Nishikawa, F. Yamashita, and M. Hashida. Mannose receptor-mediated gene transfer into macrophages using novel mannosylated cationic liposomes. *Gene Ther.* 7:292–299 (2000).
23. S. Kawakami, J. Wong, A. Sato, Y. Hattori, F. Yamashita, and M. Hashida. Biodistribution characteristics of mannosylated, fuco-

sylated, and galactosylated liposomes in mice. *Biochim. Biophys. Acta* **1524**:258–265 (2000).
24. S. C. Semple, A. Chonn, and P. R. Cullis. Interactions of liposomes and lipid-based carrier systems with blood proteins: relation to clearance behaviour in vivo. *Adv. Drug Deliv. Rev.* **32**:3–17 (1998).
25. K. Ogawara, M. Nishikawa, Y. Takakura, and M. Hashida. Pharmacokinetic analysis of hepatic uptake of galactosylated bovine serum albumin in a perfused rat liver. *J. Control. Release* **50**:309–317 (1998).
26. M. R. Vist and J. H. Davis. Phase equilibria of cholesterol/ dipalmitoylphosphatidylcholine mixtures: ^{2}H nuclear magnetic resonance and differential scanning calorimetry. *Biochemistry* **29**: 451–464 (1990).
27. T.-H. Huang, C. W. B. Lee, S. K. Das Gupta, A. Blume, and R. G. Griffin. A ^{13}C and ^{2}H nuclear magnetic resonance study of phosphatidylcholine/cholesterol interactions: characterization of liquid-gel phases. *Biochemistry* **32**:13277–13287 (1993).
28. C. A. Hunt. Related Articles Liposomes disposition in vivo. V. Liposome stability in plasma and implications for drug carrier function. *Biochim. Biophys. Acta* **719**:450–463 (1982).
29. V. A. Slepushkin, A. I. Starov, A. G. Bukrinskaya, A. B. Imbs, M. A. Martynova, L. S. Kogtev, E. L. Vodovozova, N. G. Timofeeva, J. G. Molotkovsky, and L. D. Bergelson. Interaction of influenza virus with gangliosides and liposomes containing gangliosides. *Eur. J. Biochem.* **173**:599–605 (1988).
30. A. A. Yaroslavov, A. A. Efimova, V. I. Lobyshev, Y. A. Ermakov, and V. A. Kabanov. Reversibility of structural rearrangements in lipid membranes induced by adsorption-desorption of a polycation. *Membr. Cell Biol.* **10**:683–688 (1997).

Pharmaceutical Research, Vol. 19, No. 12, December 2002 (© 2002) *Research Paper*

Pharmacokinetics and Preventive Effects of Targeted Catalase Derivatives on Hydrogen Peroxide-Induced Injury in Perfused Rat Liver

Yoshiyuki Yabe,[1] Naoki Kobayashi,[2] Makiya Nishikawa,[1] Kiyoshi Mihara,[3] Fumiyoshi Yamashita,[1] Yoshinobu Takakura,[2] and Mitsuru Hashida[1,4]

Received May 29, 2002; accepted September 6, 2002

Purpose. To investigate the pharmacokinetics and preventive effects of liver-targeted catalase (CAT) derivatives on hepatic injury caused by reactive oxygen species.

Methods. The hepatic uptake of ^{111}In-CAT, galactosylated (Gal-), mannosylated (Man-) and succinylated (Suc-) CAT was investigated in isolated perfused rat livers in a single-pass constant infusion mode. Then, pharmacokinetic parameters were obtained by fitting equations derived from a one-organ pharmacokinetic model to the outflow profile. Their effects in preventing hydrogen peroxide-induced injury were determined by lactate dehydrogenase (LDH) release from the perfused liver.

Results. The extraction of CAT derivatives by the liver was dose-dependent, and increased by the chemical modifications described. After being bound to the cell surface, chemically modified CAT derivatives were internalized by the liver faster than CAT. Pre-perfusion of a CAT derivative significantly reduced LDH release by hydrogen peroxide at least for 30 min, and Man-CAT and Suc-CAT effectively inhibited this release.

Conclusions. Internalized CAT derivatives are also effective in degrading hydrogen peroxide and targeted delivery of CAT to liver nonparenchymal cells by mannosylation or succinylation is a useful method for the prevention of hepatic injury caused by reactive oxygen species.

KEY WORDS: catalase; pharmacokinetics; perfused rat liver; chemical modification; reactive oxygen species.

INTRODUCTION

There is a great deal of evidence to suggest that reactive oxygen species (ROS) are implicated in the pathogenesis of many diseases, including atherosclerosis, cancer and Alzheimer's disease (1–3). Therefore, antioxidant enzymes such as catalase (CAT) and superoxide dismutase (SOD) have been considered as therapeutic agents for ROS-mediated injuries and diseases. In a series of studies, we have demonstrated that bovine liver CAT rapidly accumulates in hepatocytes (or liver parenchymal cells; PC) after intravenous injection (4). We developed several derivatives of CAT and SOD by chemically modifying them in order to control their pharmacokinetic behavior (5,6). It has been shown that targeted delivery of SOD and CAT to liver nonparenchymal cells (NPC) through receptor-mediated endocytosis is a promising approach to prevent hepatic ischemia/reperfusion injury (6–8). However, the major fraction of these enzyme derivatives taken up by cells via receptor-mediated endocytosis is normally transferred to and degraded in lysosomes. The binding and internalization characteristics of these chemically modified enzymes, as far as liver cells are concerned, should depend on the physicochemical properties of the ligand and the receptor involved in the uptake. To obtain the maximal therapeutic effects following delivery of these enzymes, the spatial and temporal relationships between the enzyme delivery and ROS production need to be quantitatively examined.

In this study, the hepatic disposition characteristics of ^{111}In-CAT derivatives were investigated in isolated perfused rat livers. The venous outflow patterns of these derivatives were analyzed based on a one-organ pharmacokinetic model including the binding and internalization processes to obtain the binding constant, maximum binding site and internalization rate of each derivative. Then, the inhibitory effects of pre-treatment with CAT derivatives on hydrogen peroxide (H_2O_2)-induced hepatic injury were evaluated by measuring lactate dehydrogenase (LDH) release to the outflow medium of the perfused liver. Based on the results obtained, targeted delivery of CAT to liver NPC was revealed to be an effective approach to inhibit hepatic injury caused by H_2O_2.

MATERIALS AND METHODS

Animals

Male Wistar rats (180–220 g) were purchased from the Shizuoka Agricultural Cooperative Association for Laboratory Animals (Shizuoka, Japan). All animal experiments were carried out in accordance with the Principles of Laboratory Animal Care as adopted and promulgated by the US National Institutes of Health and with the Guideline for Animal Experiments of Kyoto University.

Chemicals

Bovine liver CAT was purchased from Sigma Chemical (St. Louis, MO, USA). CAT was subjected to gel filtration

[1] Department of Drug Delivery Research, Graduate School of Pharmaceutical Sciences, Kyoto University, Sakyo-ku, Kyoto 606-8501, Japan.

[2] Department of Biopharmaceutics and Drug Metabolism, Graduate School of Pharmaceutical Sciences, Kyoto University, Sakyo-ku, Kyoto 606-8501, Japan.

[3] Department of Biopharmaceutics, Meiji Pharmaceutical University, 2-522-1 Noshio, Kiyose, Tokyo 204-8588, Japan.

[4] To whom correspondence should be addressed. (e-mail: hashidam@pharm.kyoto-u.ac.jp)

ABBREVIATIONS: AUC, the area under the plasma concentration-time curve; BSA, bovine serum albumin; CAT, catalase; C_b, inflow concentration; C_{in}, concentration in the perfusate before passing through the liver; CL_h, hepatic clearance; C_{out}, concentration in the perfusate after passing through the liver; C_s, sinusoidal concentration; CL_{total}, total body clearance; CL_{liver}, hepatic uptake clearance; DTPA, diethylenetriaminepentaacetic acid; E_{ss}, the extraction ratio; Gal-CAT, galactosylated CAT; K, binding constant; k_{int}, internalization rate constant; LDH, lactate dehydrogenase; Man-CAT, mannosylated CAT; NPC, liver nonparenchymal cells; PC, liver parenchymal cells; Q, flow rate; ROS, reactive oxygen species; SOD, superoxide dismutase; Suc-CAT, succinylated CAT; V_s, sinusoidal volume; X, binding amount; X_∞, maximum binding amount.

0724-8741/02/1200-1815/0 © 2002 Plenum Publishing Corporation

chromatography and only the fractions containing tetramer of the subunits with a molecular weight of about 240 kDa were used in the experiments (4). Diethylenetriaminepentaacetic acid (DTPA) anhydride was purchased from Dojindo Laboratory, Kumamoto, Japan. ^{111}Indium chloride ([^{111}In]$InCl_3$) was supplied by Nihon Medi-Physics Co., Takarazuka, Japan. All other chemicals were of the highest grade available.

Synthesis and Characterization of CAT Derivatives

Galactosylated (Gal-), mannosylated (Man-) and succinylated (Suc-) CAT derivatives were synthesized by the method reported previously (6). About 70% of the total protein amino groups were used for chemical modification in all derivatives. The enzymatic activity of CAT derivatives was measured by monitoring their ability to degrade hydrogen peroxide (9) and satisfactory enzymatic activity (>86% of each unmodified enzyme; 86, 90 and 97% of the original activity for Suc-CAT, Gal-CAT, and Man-CAT, respectively) was found to remain after each modification. For disposition experiments, CAT derivatives were radiolabeled with ^{111}In using DTPA anhydride as reported previously (10).

In Vivo Disposition Experiment

Rats were anesthetized by intraperitoneal injection of sodium pentobarbital (20 mg/kg). The bile duct and urinary bladder were canulated to allow the collection of bile and urine, respectively. A bolus injection of a solution of ^{111}In-CAT was made into the femoral vein at a dose of 0.1, 1, or 10 mg/kg. At given periods after injection, blood samples (0.2 ml) were withdrawn from the jugular vein over 2 h and centrifuged at 2,000 g for 2 min to obtain plasma. At 2 h after injection, the kidney, liver, spleen, heart, and lung were excised, rinsed with saline and weighed. ^{111}In-radioactivity in the plasma and organs was counted with a well-type NaI scintillation counter (ARC-500, Aloka, Tokyo, Japan). The ^{111}In-radioactivity concentration in plasma was normalized to the % of dose/ml and the area under the plasma concentration-time curve (AUC) for the experimental period or for infinite time was estimated by fitting an equation to the plasma concentration data using the non-linear least-square program MULTI (11). Total body clearance (CL_{total}) and apparent hepatic uptake clearance (CL_{liver}) were calculated by, respectively, dividing the administered dose and the amount in the liver at 2 h after administration by the AUC, as reported previously (12).

Liver Perfusion Experiment

The *in situ* liver perfusion experiments were performed as reported previously (13,14). Briefly, the liver was perfused in a single-pass mode at a flow rate of 13 ml/min with Krebs–Ringer bicarbonate buffer with 10 mM glucose, which was oxygenated with 95% O_2-5% CO_2, adjusted to pH 7.4 and incubated at 37°C. To prevent interactions between CAT derivatives and blood components, perfusate without red blood cells nor albumin was used. After conditioning the perfused liver for 20 min, ^{111}In-CAT derivatives dissolved in the perfusate were continuously infused at concentrations of 0.1, 1, 10 μg/ml. The venous outflow and the bile were collected into weighed tubes at appropriate intervals. The viability of the liver was checked with respect to both the bile flow and the LDH activity in the out flow. In all experiments, perfused livers remained viable during the course of the study. From the venous outflow curves, the extraction ratio (E_{ss}) and the hepatic clearance (CL_h) at steady- state for ^{111}In-CAT derivatives are calculated as follows:

$$E_{ss} = \frac{C_{in} - C_{out}}{C_{in}} \quad (1)$$

$$CL_h = E_{ss} Q \quad (2)$$

where C_{in} and C_{out} are the concentrations of ^{111}In-compounds in the perfusate before and after passing through the liver under steady-state conditions, and Q is the perfusion rate.

Pharmacokinetic Analysis

The outflow curves of ^{111}In-CAT derivatives in the liver perfusion system were analyzed by the one-organ pharmacokinetic model shown as Fig.1 (15). The sinusoidal compartment including the Disse space is assumed to be under well-stirred conditions, and the concentration is assumed to be identical to that in the outflow (C_s). The terms C_s and C_b correspond to C_{out} and C_{in}, respectively, in Eq. (1). The binding compartment is characterized by a maximum binding amount (X_∞) and a binding constant (K), where rapid equilibration is assumed to occur between the sinusoidal and binding compartments. This assumption of rapid equilibrium was confirmed by our previous studies where chemically modified albumin derivatives were used (14,15). V_s represents the sum of the volumes of the sinusoid and Disse spaces and this was estimated to be 0.180 ml/g liver (16).

The internalization process is assumed to follow first-order rate kinetics, the internalization rate (dX/dt) is expressed as a product of a binding amount X and its rate constant (k_{int}). The efflux of radioactivity after internalization was neglected since radioactive metabolites of ^{111}In-labeled ligands using DTPA cannot easily pass through biologic membranes (17,18). Then, in the sinusoidal and binding compartments, a mass-balance equation can be defined as follows:

$$V_s \cdot \left(\frac{dC_s}{dt}\right) + \left(\frac{dX}{dt}\right) = QC_b - QC_s - k_{int}X \quad (3)$$

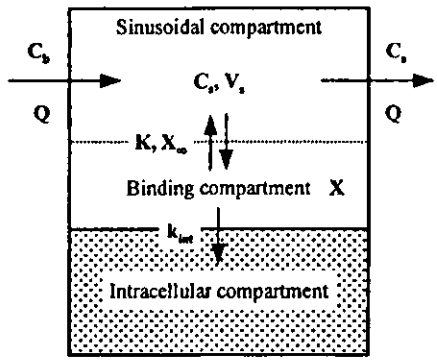

Fig. 1. Physiologic pharmacokinetic model for analyzing the hepatic uptake of ^{111}In-CAT derivatives. Q, flow rate (ml/min); C_b, inflow concentration (μg/ml); C_s, sinusoidal concentration (μg/ml); V_s, sinusoidal volume (ml); X, binding amount (μg/liver); X_∞, maximum binding amount (μg/liver); K, binding constant (ml/μg); k_{int}, internalization rate constant (min^{-1}).

The binding of ^{111}In-CAT derivatives to the cell surface is assumed to be consistent with the Langmuir equation and so the following expression holds:

$$X = \frac{X_\infty K C_s}{1 + K C_s} \quad (4)$$

Differentiated with respect to t, Eq. (4) can be rearranged to

$$\frac{dX}{dt} = \frac{X_\infty K}{(1 + K C_s)^2} \cdot \left(\frac{dC_s}{dt}\right) \quad (5)$$

Substituting Eq. 3 with Eq. (5) gives the following equation:

$$\left(V_s + \frac{X_\infty K}{(1 + K C_s)^2}\right)\left(\frac{dC_s}{dt}\right) = Q C_b - Q C_s - k_{int} \frac{X_\infty K C_s}{1 + K C_s} \quad (6)$$

The differential equations derived from Eq. (6) for various inflow concentrations are numerically solved using the Runge-Kutta-Gill method. An initial condition is $C_s = 0$ when t = 0. Curve fitting of the equations to the outflow curves was conducted using the MULTI(RUNGE) program (19) on a mainframe computer on the Kyoto University Data Processing Center.

Treatment of Perfused Liver with H_2O_2 and CAT Derivatives

The isolated rat liver was perfused in a similar way to that described above. After a stabilization period of 20 min, CAT derivative dissolved in the perfusate (500 U/ml) was infused into the liver for 30 min. The concentration of each derivative ranged from 11.4 to 13.2 μg/ml (11.4, 11.8, 12.6 and 13.2 μg/ml for CAT, Man-CAT, Gal-CAT and Suc-CAT, respectively), calculated based on the remaining CAT activity (6). Then, 0.5 mM H_2O_2 dissolved in the perfusate was continuously infused for 60 min. The venous outflow samples were collected every 10 min and the lactate dehydrogenase (LDH) activity in the outflow samples was determined using a commercial kit (LDH-UV test Wako, Wako Pure Chemicals, Japan).

Statistical Analysis

Differences were statistically evaluated by one-way analysis of variance followed by the Fisher's PLSD test at a significance level of $p < 0.05$.

RESULTS

In Vivo Disposition and Clearances of ^{111}In-CAT after Intravenous Injection in Rats

Figure 2a shows the plasma concentration-time courses of radioactivity after intravenous injection of ^{111}In-CAT into rats at different doses. ^{111}In-CAT was rapidly cleared from plasma after injection at doses of 0.1 and 1 mg/kg. Increasing the dose to 10 mg/kg, however, reduced the elimination rate of ^{111}In-CAT. Fig. 2b. shows the cumulative amounts of radioactivity in tissues, bile and urine after intravenous injection of ^{111}In-CAT. Most of the radioactivity was recovered in the liver, and little radioactivity (less than 2.5% of the dose) was recovered in other samples. Radioactivity excreted in bile gradually increased with time, and increasing the dose to 10 mg/kg resulted in a reduced biliary excretion rate (Fig. 2c).

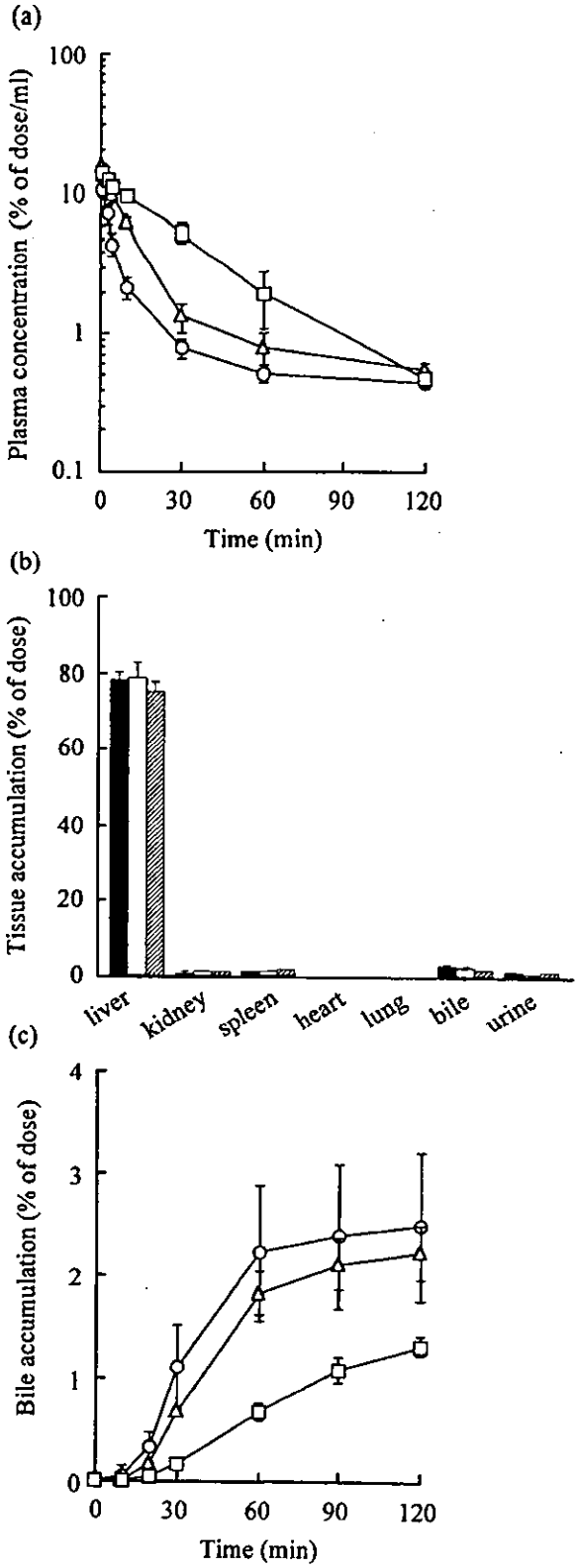

Fig. 2. (a) Plasma concentration of ^{111}In-CAT after intravenous injection in mice at doses of 0.1 mg/kg (○), 1 mg/kg (△) or 10 mg/kg (□). (b) Tissue accumulation of ^{111}In-CAT at 2h after intravenous injection in mice at a dose of 0.1 mg/kg (closed column), 1 mg/kg (open column), and 10 mg/kg (hatched column). (c) Accumulation of radioactivity in the bile after intravenous administration of ^{111}In-CAT to rats at doses of 0.1 mg/kg (○), 1 mg/kg (△) or 10 mg/kg (□). Results are expressed as the mean ± SD of at least three rats.

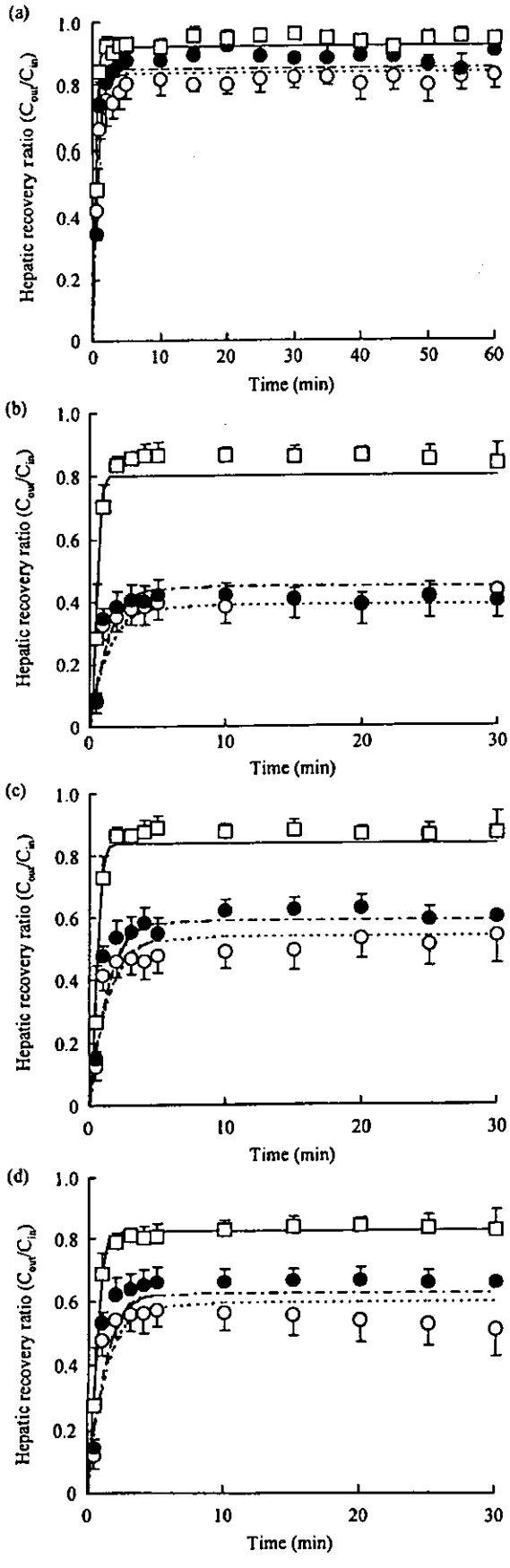

Fig. 3. Hepatic recovery ratio (C_{out}/C_{in})-time profiles of ^{111}In-CAT derivatives in the single-pass liver perfusion experiments at an inflow concentration of 0.1 μg/ml (○), 1 μg/ml (●) or 10 μg/ml (□). Values are expressed as the mean ± SD of at least three experiments. (a) CAT, (b) Gal-CAT, (c) Man-CAT, (d) Suc-CAT. Curves show simulated functions obtained based on the parameters shown in Table I. (dotted line) 0.1 μg/ml, (broken line) 1 μg/ml, (solid line) 10 μg/ml.

At any dose, the hepatic uptake clearance (CL_{liver}) accounted for more than 75% of the total body clearance (CL_{total}) (data not shown), indicating that the liver is the main organ determining the *in vivo* distribution of ^{111}In-CAT. These results are consistent with our previous results obtained in mice (4).

Hepatic Uptake of ^{111}In-CAT Derivatives during Constant Infusion in Perfused Rat Liver

Figure 3 shows the hepatic recovery ratio (C_{out}/C_{in})-time profiles of ^{111}In-CAT derivatives at various inflow concentrations (0.1, 1 and 10 μg/ml). Each ^{111}In-CAT derivative was continuously extracted by the liver during the uptake steady state. The CL_h was calculated from steady-state extraction ratio (E_{ss}) and summarized in Fig. 4. The CL_h of each derivative decreased as the inflow concentration increased. At the highest inflow concentration, the E_{ss} of ^{111}In-Suc-CAT, Gal-CAT and Man-CAT was 2.8, 2.2 and 1.9 times greater than that of ^{111}In-CAT, respectively. Extraction of ^{111}In-CAT by the liver was reduced by reducing the temperature to 4°C (data not shown), suggesting that ^{111}In-CAT was internalized by the liver cells via an energy-dependent mechanism.

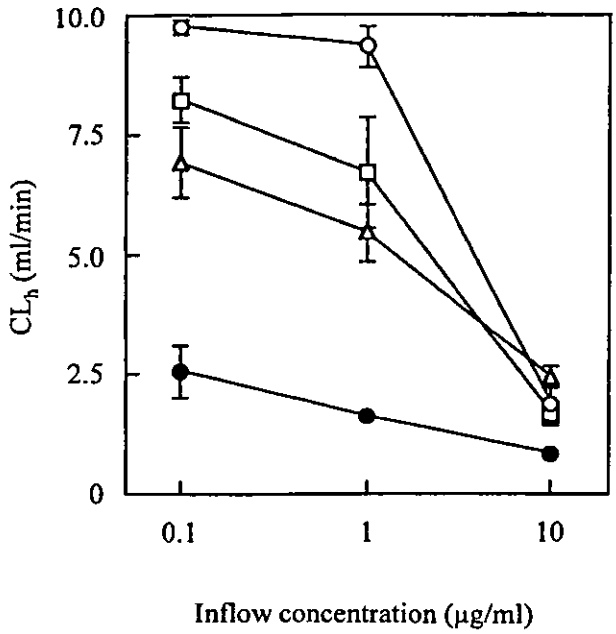

Fig. 4. Hepatic uptake clearance at steady state of ^{111}In-CAT derivatives in the single-pass liver perfusion experiments at various inflow concentrations; ●: CAT, □: Suc-CAT, ○: Gal-CAT, △: Man-CAT. Values are expressed as the mean ± SD of at least three experiments.

Analysis of Outflow Patterns Based on a Pharmacokinetic Model

The pharmacokinetic parameters of each ^{111}In-CAT derivative were estimated by fitting the mass-balance equations to the experimental results of the hepatic recovery ratio at various inflow concentrations (Table I). The maximum association amount (X_∞, μg) of each CAT derivative was relatively large compared with that of bovine serum albumin (BSA) derivatives reported previously (20). However, there were no significant differences among the CAT derivatives. Compared with ^{111}In-CAT, ^{111}In-Gal-, Man-, and Suc-CAT had a binding constant (K) that was 5.3, 3.2, and 2.1 times greater and an internalization rate (k_{int}) 2.0, 1.5, and 1.5 times greater, respectively.

Simulation curves for the hepatic recovery ratio-time profiles of ^{111}In-CAT derivatives were reconstructed employing the estimated parameters listed in Table I, and are shown in Fig. 3. In general, good agreement was observed between fitted curves and experimentally observed data at all inflow concentrations in all derivatives.

Protective Effect of CAT Derivatives against Hepatic Injury

Figure 5 shows the LDH activity in the venous outflow of the rat liver perfused with H_2O_2. When no H_2O_2 was added to the perfusate (control group), little LDH activity was detected in the venous outflow. In contrast, the LDH activity markedly increased, starting 10 min after infusion of H_2O_2-containing perfusate (no treatment group). Pretreatment with CAT resulted in a reduced LDH activity in the venous outflow. The other CAT derivatives also reduced LDH release. This effect was gradually weakened after 30 min of H_2O_2 infusion onward in the groups treated with a CAT derivative. Fig. 6 shows the cumulative LDH activity in the venous outflow for 40 min of H_2O_2 infusion. Of all the derivatives studied, Man-CAT suppressed the LDH release from the liver most efficiently, followed by Suc-CAT.

DISCUSSION

CAT is an enzyme that detoxifies hydrogen peroxide, which is involved in various ROS-mediated injuries. Therefore, treatment with CAT alone or its combination with SOD has been applied to the treatment of ROS-mediated diseases. Our recent studies have demonstrated that bovine liver CAT is rapidly delivered to liver PC (4) after intravenous injection in mice and the tissue disposition of CAT can be controlled by chemical modification (6). Furthermore, it has been shown that targeted delivery of CAT to liver NPC is a promising way to increase its potential for preventing hepatic ischemia/reperfusion injury (6,8). In order for these targeted enzymes

Table I. Pharmacokinetic Parameters for Hepatic Uptake of ^{111}In-CAT Derivatives Obtained by Model Analysis

Compound	X_∞ (μg)	K (ml/μg)	k_{int} (min^{-1})
CAT	84.4 ± 11.3	0.13 ± 0.02	0.235 ± 0.018
Gal-CAT	64.1 ± 6.0	0.69 ± 0.08	0.470 ± 0.048
Man-CAT	74.8 ± 8.1	0.42 ± 0.06	0.358 ± 0.038
Suc-CAT	94.0 ± 14.4	0.27 ± 0.05	0.357 ± 0.044

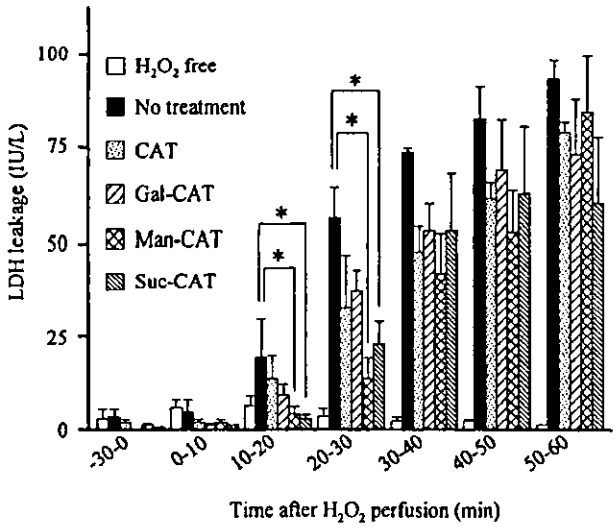

Fig. 5. LDH leakage-time profiles in the venous outflow after H_2O_2 constant infusion. Results are expressed as the mean ± SEM of at least three rats. Significantly different: *, $p < 0.05$.

to be effective against ROS-mediated injuries, they should be active after delivery to the cells. However, ligands, such as Gal-, Man- and Suc-proteins, internalized by receptor-mediated endocytosis are normally degraded within lysosomes (21,22). To design a theoretical strategy for targeted delivery of CAT to the liver in an attempt to prevent ROS-mediated injuries, the temporal and spatial disposition of CAT derivatives needs to be determined. To this end, the hepatic disposition of CAT derivatives was investigated in the isolated rat livers, because this system can give quantitative information on the binding and internalization characteristics of liver-targeted ligands (15,16,20,23).

For disposition studies, CAT derivatives were radiolabeled with ^{111}In using DTPA anhydride, because radioactive

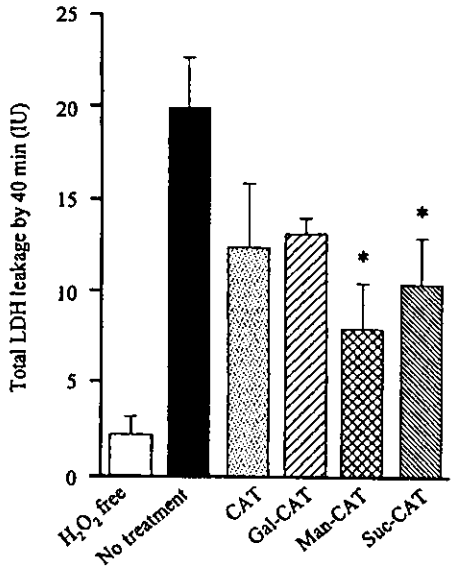

Fig. 6. Effect of pre-infusion of CAT derivatives on the accumulated LDH activity in the venous outflow 40 min after H_2O_2 constant infusion. Results are expressed as the mean ± SEM of at least three rats. Significantly different from no treatment group: *, $p < 0.05$.

metabolites, when produced after cellular uptake, are trapped within the cells where the uptake takes place (17,18). Tissue disposition studies in rats demonstrated that intravenously administered ^{111}In-CAT is rapidly eliminated from plasma and nearly 80% of the radioactivity is recovered in the liver. Increasing the dose to 10 mg/kg, however, reduced the elimination rate of ^{111}In-CAT from plasma, suggesting that CAT is taken up by the liver via a saturable process like that observed in mice (4). To quantitatively study the uptake characteristics of CAT derivatives, pharmacokinetic parameters were calculated based on the models. In the tissue distribution experiments *in vivo*, the hepatic uptake was calculated based on the amount taken up by the liver. On the other hand, the outflow profile was used to calculate the hepatic clearance in the perfusion study. To distinguish the differences, we used the two abbreviations of hepatic clearances, CL_{liver} for the *in vivo* experiments and CL_h for the *in situ* perfusion experiments.

In the perfused liver studies, ^{111}In-CAT was constantly extracted by the liver after its uptake reaching a steady state within 5 min of infusion. Furthermore, part of the radioactivity was recovered in the bile, indicating that ^{111}In-CAT is internalized into cells after binding to the cell surface. Hypoxia of the perfused liver might be concerned based on the slow perfusion of medium containing neither RBC nor albumin. However, no significant injuries caused by the simple perfusion were observed as previous studies (13–16,20,23). The E_{ss} values of ^{111}In-Gal-CAT, Man-CAT and Suc-CAT were 60.6, 50.7 and 45.4%, respectively, at the same concentration, and 2.3 to 3.0 times greater than that of ^{111}In-CAT.

We have used the model shown in Fig. 1 to analyze the pharmacokinetic characteristics of chemically modified bovine serum albumin (BSA) derivatives in the perfused rat livers (13–16,20,23). In these previous studies, the internalization rate constants (k_{int}) of BSA derivatives were experimentally obtained in addition to the model analysis; the surface bound and internalized amounts were separately measured by some means such as EDTA-wash treatment. These calculations clearly showed that the k_{int} values obtained by the model analysis were similar to those obtained experimentally, suggesting the validity of the analysis. By fitting the mass-balance equations to the outflow concentration-time profiles based on the pharmacokinetic model, the k_{int} value for Gal-, Man- and Suc-CAT was estimated to be 0.470, 0.358 and 0.357 min^{-1}, respectively, which was greater than the value for CAT (Table I). It has been reported that galactosylated, mannosylated and succinylated proteins are recognized by the asialoglycoprotein, mannose and scavenger receptors, respectively, on liver cells (24,25). The finding of greater k_{int} values for chemically modified CAT suggests that the receptor-mediated process for the hepatic uptake of modified CAT derivatives is faster than that of unmodified CAT. The k_{int} values for CAT derivatives obtained in this study were slightly different from the reported values for BSA derivatives (14,20,23). Although the reason for this discrepancy remains unknown, the CAT-specific hepatic uptake mechanism and/or differences in size and molecular weight between proteins may influence the internalization process.

The dose of CAT derivatives for the experiment to examine their preventive effects against H_2O_2 injury was adjusted in terms of the enzymatic activity to 500 U/ml, which corresponded to 11.4, 13.2, 12.6 and 11.8 μg/ml for CAT, Suc-CAT, Gal-CAT and Man-CAT, respectively. There were slight differences in the weight-based dose among CAT derivatives, but such differences could hardly affect the pharmacokinetic profiles in the perfused liver since the hepatic uptake of any CAT derivative was highly saturated at these concentrations (Fig. 4). Although pretreatment of each CAT derivative reduced the LDH release from the liver to some extent, the preventive effect did not last over 30 min (Fig. 5). The degradation of internalized ligands in the cells could explain these results. However, a series of our reports using BSA derivatives showed that the surface-bound protein derivatives are rapidly internalized (14,15,20,23). These results indicate that CAT derivatives internalized by liver cells can contribute to their protective effects against H_2O_2 injury in the perfused livers. Although the internalization rate of Suc-CAT and Man-CAT was faster than that of CAT, they were more effective than CAT in the prevention of the hepatic injury, suggesting the importance of the delivery of CAT to liver NPC. These results are comparable with our previous results on the preventive effect of CAT derivatives against hepatic ischemia/reperfusion injury (6,8).

Generally, it is known that extracellular ROS derived from Kupffer cells and polymorphonuclear leukocytes (neutrophils) play important roles in ROS-mediated hepatic injury such as ischemia/reperfusion injury (26, 27). Cellular injury to hepatocytes and endothelial cells seems to be mainly attributed to extracellular ROS rather than its intracellular counterpart. The experimental design of this study, therefore, reflects the phenomena that occur *in vivo*. Although H_2O_2 is initially localized outside cells, it can diffuse into cells to trigger oxidative reactions. Internalized CAT derivatives might prevent the reactions generated by internalized H_2O_2. The activity of endogenous antioxidant enzymes, especially CAT, in NPC is much less than in hepatocytes (28, 29), which suggests that the endothelial cells are much more susceptible to ROS than hepatocytes. Man-CAT or Suc-CAT can supplement CAT activity in hepatic endothelial cells. The present results confirm that targeted delivery of CAT to liver NPC is effective.

In conclusion, the pharmacokinetics of the hepatic uptake of CAT derivatives was determined in perfused rat liver, showing that chemically modified CAT derivatives are more rapidly internalized by liver cells than CAT. CAT derivatives targeted to liver NPC are more effective in preventing H_2O_2-induced hepatic injury. It has been shown that not only the surface- bound CAT derivative but also its counterpart internalized by receptor-mediated endocytosis is effective in preventing injury. These findings provide useful information to assist in the design and application of CAT derivatives to a range of ROS-mediated injuries.

ACKNOWLEDGMENTS

This study is being supported in part by a Grant-in-Aid for Scientific Research from the Ministry of Education, Culture, Sports, Science, and Technology of Japan.

REFERENCES

1. B. Halliwell and J. M. C. Gutteridge. Role of free radicals and catalytic metal ions in human diseases: An overview. *Methods Enzymol.* **186**:1–85 (1990).
2. P. A. Cerutti. Oxidant stress and carcinogenesis. *Eur. J. Clin. Invest.* **21**:1–5 (1991).

3. N. A. Simonian and J. T. Coyle. Oxidative stress in neurodegenerative diseases. *Annu. Rev. Pharmacol. Toxicol.* **36**:83–106 (1996).
4. Y. Yabe, Y. Koyama, M. Nishikawa, Y. Takakura, and M. Hashida. Hepatocyte-specific distribution of catalase and its inhibitory effect on hepatic ischemia/reperfusion injury in mice. *Free Radic. Res.* **30**:265–274 (1999).
5. T. Fujita, M. Nishikawa, C. Tamaki, Y. Takakura, M. Hashida, and H. Sezaki. Targeted delivery of human recombinant superoxide dismutase by chemical modification with mono- and polysaccharide derivatives. *J. Pharmacol. Exp. Ther.* **263**:971–978 (1992).
6. Y. Yabe, M. Nishikawa, A. Tamada, Y. Takakura, and M. Hashida. Targeted delivery and improved therapeutic potential of catalase by chemical modification: combination with superoxide dismutase derivatives. *J. Pharmacol. Exp. Ther.* **289**:1176–1184 (1999).
7. T. Fujita, H. Furitsu, M. Nishikawa, Y. Takakura, H. Sezaki, and M. Hashida. Therapeutic effects of superoxide dismutase derivatives modified with mono- or polysaccharides on hepatic injury induced by ischemia/reperfusion. *Biochem. Biophys. Res. Commun.* **189**:191–196 (1992).
8. Y. Yabe, N. Kobayashi, T. Nishihashi, R. Takahashi, M. Nishikawa, Y. Takakura, and M. Hashida. Prevention of neutrophil-mediated hepatic ischemia/reperfusion injury by superoxide dismutase and catalase derivatives. *J. Pharmacol. Exp. Ther.* **298**: 894–899 (2001).
9. R. F. Beers Jr. and I. W. Sizer. A spectrophotometric method for measuring the breakdown of hydrogen peroxide by catalase. *J. Biol. Chem.* **195**:133–140 (1952).
10. D. Hnatowich, W. W. Layne, and R. L. Childs. The preparation and labeling of DTPA-coupled albumin. *J. Appl. Radiat. Isot.* **12**:327–332 (1982).
11. K. Yamaoka, Y. Tanigawara, T. Nakagawa, and T. Uno. A pharmacokinetic analysis program (MULTI) for microcomputer. *J. Pharmacobio-Dyn.* **4**:879–885 (1981).
12. Y. Takakura, A. Takagi, M. Hashida, and H. Sezaki. Disposition and tumor localization of mitomycin C-dextran conjugates in mice. *Pharm. Res.* **4**:293–300 (1987).
13. K. Nishida, C. Tonegawa, C. Kakutani, M. Hashida, and H. Sezaki. Statistical moment analysis of hepatobiliary transport of phenol red in the perfused liver. *Pharm. Res.* **6**:140–146 (1989).
14. H. Furitsu, K. Ogawara, T. Fujita, F. Yamashita, Y. Takakura, H. Sezaki, and M. Hashida. Pharmacokinetic analysis of scavenger receptor-mediated uptake of anionized proteins in the isolated perfused rat liver. *Int. J. Pharm.* **151**:15–26 (1997).
15. K. Nishida, T. Takino, Y. Eguchi, F. Yamashita, M. Hashida, and H. Sezaki. Pharmacokinetic analysis of uptake process of lactosaminated albumin in rat liver constant infusion experiments. *Int. J. Pharm.* **80**:101–108 (1992).
16. K. Nishida, C. Tonegawa, S. Nakane, Y. Takakura, M. Hashida, and H. Sezaki. Effect of electric charge on the hepatic-uptake of macromolecules in the rat-liver. *Int. J. Pharm.* **65**:7–17 (1990).
17. Y. Arano, T. Mukai, T. Uezono, K. Wakisaka, H. Motonari, H. Akizawa, Y. Taoka, and A. Yokoyama. A biological method to evaluate bifunctional chelating agents to label antibodies with metallic radionuclides. *J. Nucl. Med.* **35**:890–898 (1994).
18. J. R. Duncan and M. J. Welch. Intracellular metabolism of indium-111-DTPA-labeled receptor targeted proteins. *J. Nucl. Med.* **34**:1728–1738 (1993).
19. K. Yamaoka and T. Nakagawa. A nonlinear least squares program based on differential equations, MULTI (RUNGE), for microcomputers. *J. Pharmacobio-Dyn.* **6**:595–606 (1983).
20. K. Ogawara, S. Hasegawa, M. Nishikawa, Y. Takakura, and M. Hashida. Pharmacokinetic evaluation of mannosylated bovine serum albumin as a liver cell-specific carrier: quantitative comparison with other hepatotropic ligands. *J. Drug Target.* **6**:349–360 (1999).
21. K. Bridges, J. Harford, G. Ashwell, and R. D. Klausner. Fate of receptor and ligand during endocytosis of asialoglycoproteins by isolated hepatocytes. *Proc. Natl. Acad. Sci. USA* **79**:350–354 (1982).
22. P. D. Stahl, P. H. Schlesinger, E. Sigardson, J. S. Rodman, and Y. C. Lee. Receptor-mediated pinocytosis of mannose glycoconjugates by macrophages: Characterization and evidence for receptor recycling. *Cell* **19**:207–215 (1980).
23. K. Ogawara, M. Nishikawa, Y. Takakura, and M. Hashida. Pharmacokinetic analysis of hepatic uptake of galactosylated bovine serum albumin in a perfused liver. *J. Control. Release* **50**:309–317 (1998).
24. M. Nishikawa, Y. Ohtsubo, J. Ohno, T. Fujita, Y. Koyama, F. Yamashita, M. Hashida, and H. Sezaki. Pharmacokinetics of receptor-mediated hepatic uptake of glycosylated albumin in mice. *Int. J. Pharm.* **85**:75–85 (1992).
25. Y. Takakura, T. Fujita, H. Furitsu, M. Nishikawa, H. Sezaki, and M. Hashida. Pharmacokinetics of succinylated proteins and dextran sulfate in mice: Implications for hepatic targeting of protein drugs by direct succinylation via scavenger receptors. *Int. J. Pharm.* **105**:19–29 (1994).
26. H. Jaeschke. Reactive oxygen and ischemia/reperfusion injury of the liver. *Chem-Biol. Interact.* **79**:115–136 (1991).
27. H. Jaeschke, A. P. Bautista, Z. Spolarics, and J. J. Spitzer. Superoxide generation by Kupffer cells and priming neutrophils during reperfusion after hepatic ischemia. *Free Radic. Res. Commun.* **15**:277–284 (1991).
28. I. Hamer, R. Wattiaux, and S. W. D. Coninck. Deleterious effects of xanthine oxidase on rat liver endothelial cells after ischemia/reperfusion. *Biochim. Biophys. Acta* **1269**:145–152 (1995).
29. Z. Spolarics and J.-X. Wu. Role of glutathione and catalase in H_2O_2 detoxification in LPS-activated hepatic endothelial and Kupffer cells. *Am. J. Physiol.* **273**:G1304–G1311 (1997).

0022-3565/02/3012-467–477$7.00
THE JOURNAL OF PHARMACOLOGY AND EXPERIMENTAL THERAPEUTICS
Copyright © 2002 by The American Society for Pharmacology and Experimental Therapeutics
JPET 301:467–477, 2002

Vol. 301, No. 2
4659/981644
Printed in U.S.A.

Pharmacokinetic Analysis of in Vivo Disposition of Succinylated Proteins Targeted to Liver Nonparenchymal Cells via Scavenger Receptors: Importance of Molecular Size and Negative Charge Density for in Vivo Recognition by Receptors

YASUOMI YAMASAKI, KAZUYA SUMIMOTO, MAKIYA NISHIKAWA, FUMIYOSHI YAMASHITA, KIYOSHI YAMAOKA, MITSURU HASHIDA, and YOSHINOBU TAKAKURA

Department of Biopharmaceutics and Drug Metabolism, Graduate School of Pharmaceutical Sciences, Kyoto University, Sakyo-ku, Kyoto, Japan (Y.Y., K.S., K.Y., Y.T.); Department of Drug Delivery Research, Graduate School of Pharmaceutical Sciences, Kyoto University, Sakyo-ku, Kyoto, Japan (M.N., F.Y., M.H.)

Received October 16, 2001; accepted January 17, 2002 This article is available online at http://jpet.aspetjournals.org

ABSTRACT

In vivo disposition characteristics of succinylated (Suc-) proteins were studied after intravenous injection in mice in relation to their molecular characteristics as negatively charged macromolecules. Recombinant superoxide dismutase (SOD; molecular mass, 32 kDa), bovine serum albumin (BSA; molecular mass, 67 kDa), and bovine IgG (molecular mass, 150 kDa) were used to produce succinylated derivatives with different degrees of modification. ^{111}In-labeled Suc-SODs were rapidly excreted into the urine with no significant hepatic uptake. In contrast, ^{111}In-Suc-BSA and Suc-IgG were significantly taken up by liver nonparenchymal cells via scavenger receptors (SRs) according to the degree of succinylation and the dose injected. Interestingly, highly succinylated BSAs exhibited significant accumulation in the kidney at higher doses when the hepatic uptake was saturated. Pharmacokinetic analysis demonstrated that the hepatic uptake of succinylated proteins depended on the molecular size and the estimated surface density of succinylated amino residues. Further analysis based on a physiological pharmacokinetic model, involving a saturable process with Michaelis-Menten kinetics, revealed that the surface density of negative charges was correlated with the affinity of larger succinylated proteins for the hepatic SRs. Thus, the present study has provided useful basic information for a therapeutic strategy and the molecular design of succinylated proteins for use as drug carriers and therapeutic agents per se for SR-mediated targeting in vivo.

Site-specific drug delivery is a very important strategy for the optimization of drug therapy in terms of efficacy and safety since the pharmacological action of the drug of interest can be targeted to a specific site in the body. Among a variety of site-specific drug delivery methods, the use of a carrier system that is recognized by specific receptors on the target cells is one of the most powerful tools for targeted delivery of a variety of therapeutic agents, including chemotherapeutic compounds, protein drugs, antisense oligonucleotides, and genes (Takakura and Hashida, 1996; Wang and Low, 1998; Smith and Wu, 1999).

Scavenger receptors (SRs), which can recognize anionic macromolecules with unusually broad but circumscribed ligand specificity, are expressed on liver nonparenchymal cells (endothelial and Kupffer cells) and various macrophages (Linehan et al., 2000). The ligands for the SRs involve negatively charged proteins, such as maleylated and succinylated albumins, modified low-density lipoproteins, and polynucleotides (Terpstra et al., 2000). In particular, negatively charged albumins have been used as drug carriers via SRs. Successful receptor-mediated delivery to macrophages in vitro has been achieved with low-molecular-weight antitumor agents conjugated with maleylated albumin (Mukhopadhyay et al., 1992, 1995; Basu et al., 1994). Recently, maleylated albumin has also been used as a targeting carrier for a photosensitizer (Nagae et al., 1998) and a macrophage-activating peptide (Srividya et al., 2000a,b) via SRs. In addition, SR-mediated endocytosis has been used to deliver proteins as antigens. Several studies have shown that the immunological characteristics of proteins can be modulated by maleylation (Abraham et al., 1995, 1997; Singh et al., 1998; Bansal et al., 1999; Nicoletti et al., 1999). In addition, succinylated or other negatively charged albumins are interesting compounds since they exhibit antiviral effects (Jansen

ABBREVIATIONS: SR, scavenger receptor; SOD, superoxide dismutase; BSA, bovine serum albumin; FITC, fluorescein isothiocyanate; poly I, polyinosinic acid; poly C, polycytidylic acid; PAGE, polyacrylamide gel electrophoresis; DTPA, diethylenetriaminepentaacetic acid; Suc-, succinylated; PI, propidium iodide; vWF, von Willebrand factor; AUC, area under the curve; CL, clearance; PP, plasma pool; EC, sinusoidal and Disse spaces; IC, intracellular space; SRA, class AI/AII SRs.

et al., 1993; Kuipers et al., 1997). Moreover, we have recently demonstrated that targeted delivery to liver nonparenchymal cells and improved therapeutic effects of catalase can be achieved by direct succinylation of the enzyme (Yabe et al., 1999).

In spite of the therapeutic potential of the delivery approach based on an SR-mediated mechanism, the relationship between the physicochemical characteristics of negatively charged proteins, such as the molecular weight and number of negative charges, and their in vivo pharmacokinetic profiles are not yet fully understood. Therefore, the purpose of the present study was to clarify this relationship to establish a strategy for the rational design of negatively charged proteins as drug carriers and for therapeutic purposes.

Three kinds of model proteins, recombinant superoxide dismutase (SOD), bovine serum albumin (BSA), and bovine IgG were selected and used to prepare succinylated derivatives with different degrees of modification. The pharmacokinetic characteristics of these succinylated proteins were studied after systemic administration of various doses to mice. The in vivo distribution properties of the succinylated proteins were analyzed and discussed in relation to their molecular characteristics as negatively charged proteins.

Materials and Methods

Animals. Male ddY mice (25–27 g) were purchased from the Shizuoka Agricultural Cooperative Association for Laboratory Animals (Shizuoka, Japan). Animals were maintained under conventional housing conditions.

Chemicals. BSA, IgG, fluorescein isothiocyanate (FITC), polyinosinic acid (poly I) and polycytidylic acid (poly C) were purchased from Sigma Chemical (St. Louis, MO). Rabbit anti-human von Willebrand factor antisera and rhodamine conjugated donkey anti-rabbit IgG were purchased from DAKO Japan (Kyoto, Japan) and Chemicon International, Inc. (Temecula, CA), respectively. Recombinant human SOD was supplied by Asahi Kasei (Tokyo, Japan). Succinic anhydride was obtained from Nacalai Tesque (Kyoto, Japan). [^{111}In]Indium chloride was supplied by Nihon Medi-Physics (Takarazuka, Japan). All other chemicals were obtained commercially as reagent-grade products.

Synthesis and Characterization of Succinylated Proteins. Succinylated proteins with various degrees of modification were synthesized by reacting different amounts of succinic anhydride with the ϵ-NH_2 group of the lysine residues of proteins according to a previously described method (Takakura et al., 1994). In brief, each protein was dissolved in 0.2 M Tris buffer, pH 8.65, and an appropriate amount of succinic anhydride was added. The mixture was stirred for 12 h at room temperature. The succinylated proteins were then washed by dialysis, concentrated by ultrafiltration, and lyophilized. The number of free amino acid groups was determined by trinitrobenzene sulfonic acid using glycine as a standard to estimate the degree of modification (Habeeb, 1966). The molecular masses of the succinylated proteins were estimated by SDS-PAGE. Myosin (mol. wt., 220,000), phosphorylase (mol. wt., 97,400), BSA (mol. wt., 66,000), ovalbumin (mol. wt., 46,000), carbonic anhydrase (mol. wt., 30,000), trypsin inhibitor (mol. wt., 21,500), and lysozyme (mol. wt., 14,300) were used as molecular weight markers. The homogeneity of synthesized proteins was ascertained from the results of SDS-PAGE. The bands of succinylated proteins were very sharp and shifted upward with increasing the degree of succinylation (data not shown). The SDS-PAGE analysis also showed that polymerization of synthesized proteins was negligible. The apparent surface density of the succinylated amino groups was determined by dividing the number of succinylated amino groups by the accessible surface area of the succinylated protein calculated from the following equation: (accessible surface area) = 6.3 (molecular mass)$^{0.73}$ (Miller et al., 1987). The electrophoretic mobility of the succinylated proteins was determined using a laser electrophoresis-zeta potential analyzer (LEZA-500T, Otsuka Electronics).

Radiolabeling and Fluorescein-Labeling of Succinylated Proteins. For the in vivo disposition experiments, proteins were radiolabeled with ^{111}In using the bifunctional chelating agent DTPA anhydride according to the method of Hnatowich et al. (1982). Briefly, each succinylated protein (5 mg) was dissolved in 1 ml of 0.1 M HEPES buffer, pH 7.0, and mixed with 2- or 3-fold molar amounts of DTPA anhydride in 20 μl of dimethyl sulfoxide. The mixture was stirred for 1 h at room temperature and purified by gel filtration, using a Sephadex G-25 column to remove the unreacted DTPA. The protein derivative fractions were collected and concentrated by ultrafiltration. Then, 20 μl of $^{111}InCl_3$ solution (74 MBq/ml) was added to 20 μl of 1 M sodium acetate, and 60 μl of DTPA-coupled derivative solution was added to the mixture. After 30 min, the mixture was purified by gel filtration using a PD-10 column and by eluting with 0.1 M acetate buffer, pH 6.0. The derivative fractions were collected and concentrated by ultrafiltration. This radiolabeling method is suitable for examining the distribution phase of macromolecules from plasma to various tissues because any radioactive metabolites produced after cellular uptake are retained within the cells where the uptake takes place (Duncan and Welch, 1993; Arano et al., 1994). For confocal microscopic studies, Suc_{54}-BSA was labeled with FITC by the method of Monsigny et al. (1984). In brief, 1 μmol of Suc_{54}-BSA was dissolved in 10 ml of 0.1 M sodium carbonate buffer, pH 9.5, and then 3 μmol of FITC was added to the solution, followed by stirring for 5 h at room temperature. The mixture was purified by gel filtration using a PD-10 column, eluting with *n*-butanol/water (5:95), and dialysis and then concentrated by ultrafiltration and lyophilized.

In Vivo Disposition Experiments. ^{111}In-labeled succinylated proteins were injected into the tail vein of male ddY mice at doses of 0.1, 1, 10, and 20 mg/kg. At appropriate times after administration, blood was collected from the vena cava under ether anesthesia, and the mice were sacrificed. Heparin sulfate was used as an anticoagulant. Plasma was obtained from the blood by centrifugation. The kidney, spleen, liver, lung, and heart were removed, rinsed with saline, and weighed. The amount of ^{111}In radioactivity in urine was also determined by collecting the excreted urine and that remaining in the bladder. The radioactivity in each sample was counted using a well-type NaI-scintillation counter (ARC-500; Aloka, Tokyo, Japan). Contamination by plasma in each tissue sample was corrected using the distribution data for ^{111}In-BSA after intravenous injection, assuming that BSA was not taken up by the tissue during the 10-min period.

For competition experiments, ^{111}In-labeled Suc_{54}-BSA (0.1 mg/kg) was injected into mice 1 min after injection of poly I, poly C, or Suc_{54}-BSA at the dose of 10 mg/kg. Ten minutes after injection of ^{111}In-labeled Suc_{54}-BSA, the liver and kidney were collected and subjected to radioactivity counting as described.

Confocal Microscopic Studies. To examine the cellular localization in the liver and kidney, FITC-Suc_{54}-BSA was administered intravenously to mice at a dose of 20 mg/kg. At 10 min after administration, mice were sacrificed; saline was infused via the portal vein to remove blood, and the liver and kidney were excised. Slices 5 μm thick were made, fixed with 20% formalin buffer. Slices were treated with RNase to avoid staining the cell components, except for the nucleus, and dyed with propidium iodide (PI) to visualize the nucleus. Liver and kidney endothelial cells were stained by a rabbit anti-human von Willebrand factor (vWF) antisera at 1:200, followed by a donkey anti-rabbit IgG rhodamine-conjugated second antibody. The slices were scanned with a confocal laser microscope (MRC-1024; Bio-Rad, Hercules, CA).

Calculation of AUC and Clearances. The plasma ^{111}In radioactivity concentrations were normalized with respect to the percent-

age of the dose per milliliter and analyzed using the nonlinear least-square program MULTI (Yamaoka et al., 1981). The tissue distribution patterns were evaluated using tissue uptake clearances according to the integration plot analysis. The tissue accumulation at time t was proportional to the AUC_{0-t}. By dividing the tissue accumulation at time t (X_t) and the AUC_{0-t} by the plasma concentration (C_t), CL_{tissue} was obtained from the slope of the plot of X_t/C_t versus AUC_{0-t}/C_t.

Pharmacokinetic Analysis Based on a Physiological Model. The time-courses of the plasma concentrations and liver accumulations of ^{111}In-labeled succinylated proteins were analyzed based on the physiological model shown in Fig. 1 (Nishikawa et al., 1995). In this model, the body is represented by three compartments [i.e., the plasma pool (PP), the sinusoidal and Disse spaces in the liver (EC), and the intracellular space in the liver (IC)]. The PP and EC compartments have apparent volumes of distribution V_p and V_l, respectively. The PP compartment represents all the plasma spaces within the blood vessels of tissues, except for the liver; it is connected with the EC by hepatic plasma flow. The uptake of succinylated protein from EC to IC is expressed as a saturable process exhibiting Michaelis-Menten kinetics, with a maximum rate of uptake, $V_{max,l}$ (nanomoles per hour), and a Michaelis constant, $K_{m,l}$ (nanomolar). Extrahepatic elimination from PP is assumed to be a saturable process represented by $V_{max,p}$ or $K_{m,p}$. At time 0, the injected substance is assumed to be distributed in the PP and EC compartments at the same concentration. Mass balance equations for the concentration of succinylated proteins in PP and EC and the amount of succinylated proteins in IC are expressed as:

$$\frac{dC_p}{dt} = \left(QC_l - QC_p - \frac{V_{max,p}}{K_{m,p} + C_p} C_p\right)/V_p \quad (1)$$

$$\frac{dC_l}{dt} = \left(QC_p - QC_l - \frac{V_{max,l}}{K_{m,l} + C_l} C_l\right)/V_l \quad (2)$$

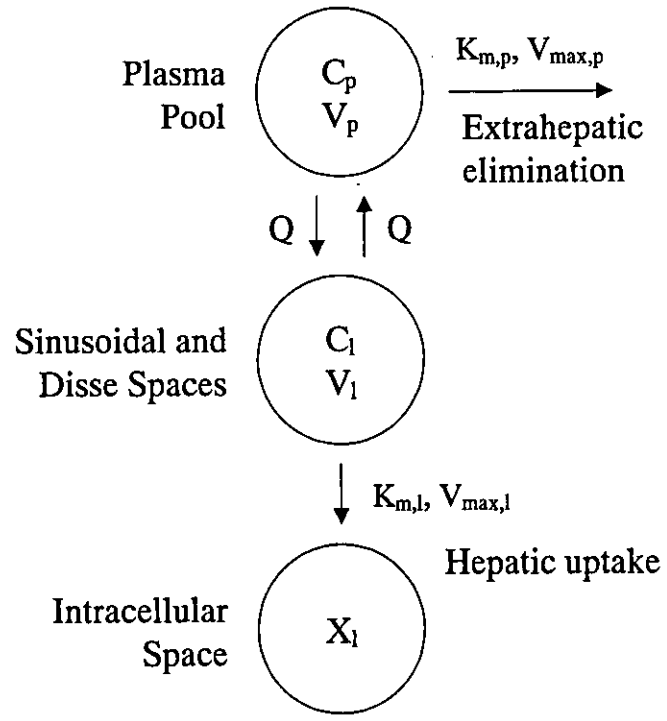

Fig. 1. Physiological pharmacokinetic model for analyzing the in vivo disposition of succinylated proteins. $K_{m,p}$ and $K_{m,l}$ are the Michaelis constants for plasma pool and liver, respectively. $V_{max,p}$ and $V_{max,l}$ are the maximum rates of uptake for plasma pool and liver, respectively. Q is the hepatic plasma flow rate.

$$\frac{dX_l}{dt} = \frac{V_{max,l}}{K_{m,l} + C_l} C_l \quad (3)$$

where C_p and C_l are the concentrations of succinylated proteins in PP and EC, respectively, X_l is the amount accumulated in IC, and Q is the hepatic plasma flow rate. The values of V_p, V_l, and Q were assumed to be 1.5 ml, 0.15 ml, and 85 ml/h, respectively (Gerlowski and Jain 1983).

To estimate the effect of the pharmacokinetic parameters on the relationship between the injected dose and tissue uptake clearance, a computer simulation was performed. Some values were substituted for the $K_{m,l}$, $K_{m,p}$, $V_{max,l}$, and $V_{max,p}$ of eqs. 1 to 3; these equations were solved by the Runge-Kutta-Gill method, and then the tissue uptake clearance was calculated.

To determine the parameters, these differential equations were simultaneously fitted to the experimental plasma concentration and liver accumulation data using the nonlinear least-squares method MULTI (Yamaoka et al., 1981) associated with the Runge-Kutta-Gill method MULTI(RUNGE) (Yamaoka and Nakagawa, 1983) on the M382 mainframe computer of Kyoto University Data Processing Center. The damping Gauss-Newton method was used as an algorithm for the nonlinear least-squares method. The plasma concentration and liver accumulation data were weighted reciprocally (i.e., $1/C_p$ and $1/X_l$).

Results

Physicochemical Characteristics of Succinylated Proteins. The physicochemical properties of the succinylated proteins are summarized in Table 1. In each protein, the number of succinylated amino groups depended on the amount of reacted succinic anhydride. Succinylation slightly increased the molecular weight determined by SDS-PAGE. The calculated surface density of the succinylated amino groups correlated with the electrical mobility determined by the laser electrophoresis-ζ-potential analyzer (r^2 = 0.7652).

Distribution of ^{111}In-Succinylated Proteins after Intravenous Injection. Figure 2 shows the time course of the plasma concentrations, liver accumulation, and kidney accumulation of ^{111}In-Suc-SODs (A–C), ^{111}In-Suc-BSAs (D–I), and ^{111}In-Suc-IgGs (J–L), with different degrees of succinylation after intravenous injection in mice together with those of unmodified proteins. ^{111}In-SOD, ^{111}In-Suc$_9$-SOD, and ^{111}In-Suc$_{22}$-SOD rapidly disappeared from the plasma circulation in a similar manner but showed no significant accumulation in the liver after administration (Fig. 2, A–C). These profiles were independent of the injected dose. However, a marked difference was observed in their renal excretion, a major elimination pathway for small proteins. Unmodified SOD and Suc$_9$-SOD exhibited significant accumulation in the kidney, which decreased with a concomitant increase in urinary excretion (data not shown) as the dose increased. However, Suc$_{22}$-SOD was mainly recovered in the urine (30% of dose) with minimal renal uptake (approximately 15% of the dose), regardless of the injected dose.

On the other hand, Suc-BSAs showed distinct biodistribution profiles according to the degree of succinylation and the administered dose (Fig. 2, E–I). ^{111}In-Suc$_{20}$-BSA remained in the blood circulation for a long time, and only a little was taken up by the liver. This profile was similar to that of ^{111}In-BSA (Fig. 2D). With an increase in the degree of succinylation, the elimination rate from the plasma circulation and the amount of Suc-BSA taken up by the liver increased, and Suc$_{40}$-BSA, Suc$_{46}$-BSA, and Suc$_{54}$-BSA all showed sim-

TABLE 1
Physicochemical characteristics of succinylated proteins

	Number of Succinylated Amino Residues[a]	Molecular Weight[b]	Estimated Surface Density of Succinylated Amino Residues[c] $\times 10^3$	Electrical Mobility[d] $\times 10^4$
	mol/mol		*molecules/Å²*	*cm²/Vs*
SOD	0	32,000	0	−0.061 ± 0.133
Suc_9-SOD	9.3	33,000	0.745	−0.191 ± 0.257
Suc_{22}-SOD	21.6	34,000	1.683	−0.582 ± 0.273
BSA	0	67,000	0	−0.353 ± 0.114
Suc_{20}-BSA	19.7	69,000	0.920	−0.588 ± 0.541
Suc_{28}-BSA	28.0	72,300	1.260	−0.946 ± 0.192
Suc_{40}-BSA	39.7	75,900	1.724	−1.277 ± 0.557
Suc_{46}-BSA	46.1	79,800	1.930	−1.672 ± 0.359
Suc_{54}-BSA	53.6	84,300	2.157	−1.912 ± 0.336
IgG	0	150,000	0	0.027 ± 0.024
Suc_{22}-IgG	22.2	165,000	0.547	−0.276 ± 0.046
Suc_{50}-IgG	49.9	177,000	1.169	−0.808 ± 0.081

[a] The numbers of succinylated amino groups were determined by the TNBS method.
[b] The molecular weights of compounds were estimated by SDS-PAGE.
[c] Surface density of succinylated amino residues was calculated by dividing the number of succinylated amino groups by the surface area of the protein.
[d] Electrical mobilities were determined using a laser electrophoresis-zeta potential analyzer (LEZA-500T). Results were expressed as mean ± S.D.

ilar profiles. The hepatic uptake seemed to be saturable since increasing the dose reduced the amount and the rate of liver accumulation. Furthermore, it was shown that highly succinylated BSAs (Suc_{40}-BSA, Suc_{46}-BSA, and Suc_{54}-BSA) were taken up by kidney, especially at higher doses, although BSA did not undergo glomerular filtration under a normal physiological condition.

A similar degree of succinylation-dependent hepatic uptake was observed for the larger protein IgG (Fig. 2, J and L). ^{111}In-Suc_{50}-IgG was taken up by the liver at a lower dose, but the rate was slower than that of highly succinylated BSA. On the other hand, ^{111}In-IgG and ^{111}In-Suc_{22}-IgG were retained in the plasma circulation for a long time after intravenous injection, without any significant accumulation in the liver. No marked renal uptake was observed for native IgG and these IgG derivatives. No significant radioactivity was recovered in any tissues other than the liver and kidney after administration of all types of succinylated protein.

Confocal Microscopic Studies. Figure 3 shows the confocal microscopic images of mouse liver (A and C) and kidney (B and D) 10 min after injection of FITC-Suc_{54}-BSA (20 mg/kg). The images in Fig. 3, A and B, are stained by PI, and the images shown in Fig. 3, C and D, are stained immunohistochemically by anti-vWF antibody. In Fig. 3A, FITC derived from Suc_{54}-BSA was localized in the cells with smaller nuclei along with the sinusoid not in the parenchymal cells with larger nuclei, indicating that FITC-Suc_{54}-BSA was selectively internalized by liver nonparenchymal cells, including endothelial and/or Kupffer cells. Immunohistochemical staining with endothelial cell-specific anti-vWF antibody showed that vWF positive cells are the major contributors for the uptake (Fig. 3C). On the other hand, vWF positive cells in the kidney were not responsible for the renal uptake of FITC-Suc_{54}-BSA (Fig. 3B and 3D). It seemed that strong fluorescein staining was observed in the luminal side of the proximal renal tubule, suggesting FITC-Suc_{54}-BSA underwent glomerular filtration and was taken up by the tubular cells, although the BSA derivatives cannot pass through the glomerular capillary wall due to size restriction.

Competition of Hepatic and Renal Uptake of ^{111}In-labeled Suc_{54}-BSA by Preadministration of Poly I, Poly C, or Suc_{54}-BSA. To determine whether ^{111}In-labeled succinylated proteins are taken up by the liver and by the kidney via specific receptors, competition studies were performed using poly I, poly C, and Suc_{54}-BSA (Fig. 4). Hepatic uptake of ^{111}In-Suc_{54}-BSA was significantly inhibited by poly I and Suc_{54}-BSA but not by poly C (Fig. 4A), indicating that succinylated proteins could be taken up by the liver via SRs. On the other hand, renal uptake of ^{111}In-Suc_{54}-BSA was not obviously inhibited by poly I and poly C, and rather Suc_{54}-BSA increased the amount of Suc_{54}-BSA in the kidney (Fig. 4B). These results show that renal uptake of succinylated proteins was independent of scavenger receptor-mediated endocytosis.

Calculation of AUC and Organ Uptake Clearances. For a quantitative comparison between the distribution profiles of the native and succinylated proteins, the clearance values for the total body (CL_{total}), liver (CL_{liver}), kidney (CL_{kidney}), and urine (CL_{urine}), as well as the AUC, were calculated based on the distribution data shown in Fig. 2 and summarized in Table 2. As far as Suc-SOD was concerned, the CL_{total} was almost independent of the injected dose, and CL_{kidney} and CL_{urine} clearances made a major contribution, although the CL_{liver} was slightly high in the case of Suc_{22}-SOD. These results suggested that glomerular filtration was a key pathway for the elimination of Suc-SOD after intravenous injection. The CL_{kidney} value of Suc_9-SOD was significantly higher than that of Suc_{22}-SOD, suggesting that Suc_9-SOD underwent more efficient tubular reabsorption. As the injected dose increased, the CL_{kidney} decreased and CL_{urine} increased, indicating that saturation of tubular uptake took place. On the other hand, in the case of Suc-BSA or Suc-IgG, the CL_{total} and CL_{liver} (the main contributor to the CL_{total}) varied depending on the degree of succinylation and the injected dose. At the lowest dose (0.1 mg/kg), Suc_{46}-BSA and Suc_{54}-BSA had a large CL_{liver} of about 70 ml/h, a value that is close to the hepatic plasma flow rate (85 ml/h) in mice, and the CL_{liver} value fell with a decrease in the number of succinylations per BSA molecule (48.0, 9.4, and 0.4 ml/h for Suc_{40}-

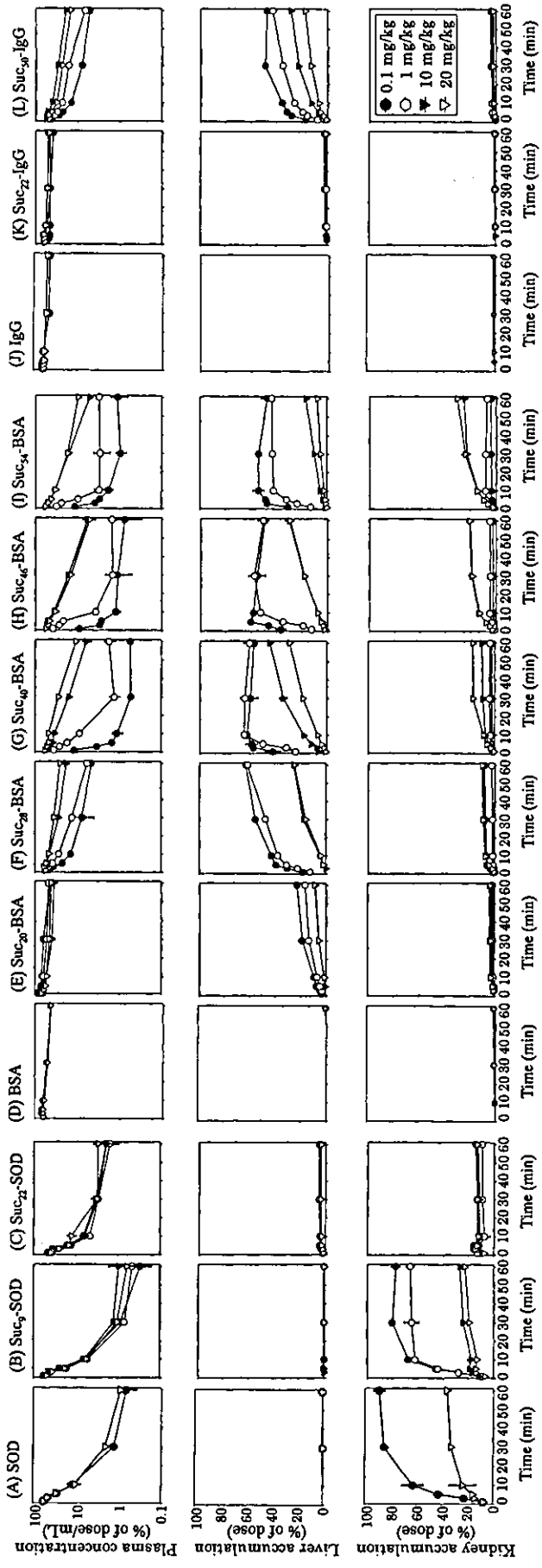

Fig. 2. Time-courses of plasma concentrations and liver and kidney accumulation of ^{111}In-labeled SOD (A), Suc_9-SOD (B), Suc_{22}-SOD (C), BSA (D), Suc_{20}-BSA (E), Suc_{28}-BSA (F), Suc_{40}-BSA (G), Suc_{46}-BSA (H), Suc_{54}-BSA (I), IgG (J), Suc_{22}-IgG (K), and Suc_{50}-IgG (L) in mice after intravenous injection of doses of 0.1 (●), 1 (○), 10 (▼), and 20 (▽) mg/kg. Results are expressed as the mean ± S. D. of three mice.

BSA, Suc_{28}-BSA, and Suc_{20}-BSA, respectively), suggesting that the degree of succinylation determines the rate of hepatic uptake. On increasing the injected dose, the CL_{liver} value for each derivative significantly decreased. Regardless of their molecular weight being greater than the threshold of glomerular filtration, Suc-BSAs with a higher degree of succinylation showed relatively large CL_{kidney} values. At the higher doses (10 and 20 mg/kg), the CL_{kidney} values for Suc_{46}-BSA and Suc_{54}-BSA were comparable with the CL_{liver}, indicating that renal uptake plays an important role in the disposition of Suc-BSAs under these conditions. Although clearances were very small for Suc_{22}-IgG, the clearance values of Suc_{50}-IgG were similar to those of Suc_{28}-BSA.

Further analysis was carried out to investigate the relationship between the physicochemical properties and disposition characteristics of the succinylated proteins. In Fig. 5, the hepatic uptake clearances of Suc-IgGs, Suc-BSAs, and Suc-SODs at the lowest dose of 0.1 mg/kg were plotted as a function of the estimated surface density of the succinylated amino groups of these proteins to compare the clearances of the succinylated proteins with different molecular weights. The CL_{liver} for succinylated catalase (molecular mass, 250 kDa), which has been shown to be effectively taken up by the liver nonparenchymal cells in our previous study (Yabe et al., 1999), was also included in Fig. 5. A good correlation was observed between the surface density of succinylated amino groups and the hepatic uptake clearance, up to a density of about 1.5×10^3 molecules/Å^2; the clearances increased in parallel with the density. Above this density, the clearance values for the liver remained almost constant. These results imply that the apparent surface density of the succinylated amino groups of modified proteins could be a determinant for recognition by SRs on liver nonparenchymal cells. The CL_{liver} value for Suc_{22}-SOD, however, did not fit this correlation. Despite its relatively high surface density of succinylated amino residues (1.68×10^3 molecules/Å^2), the CL_{liver} was low. This result suggests that the molecular weight or size of the succinylated proteins may be another important factor.

Simulation Studies Based on a Physiological Model. Before determination of the pharmacokinetic parameters in the physiological model shown in Fig. 1, computer simulation studies were carried out to ascertain theoretically the effect of the pharmacokinetic parameters in the model on the relationship between the tissue uptake clearance and injected dose. As shown in Fig. 6, when the K_m value increased from 0.1 to 500 μg/ml, the absolute value of the tissue uptake clearance became lower, and the slope of the curve became more gentle with the threshold dose for rapidly decreasing clearance shifting to a lower dose. In contrast, when the V_{max} value increased from 1 to 200 μg/h, the absolute clearance value decreased, whereas the profile of the clearance as a function of the injected dose remained almost unchanged. These computer simulation results indicate that the dose dependence of the clearance profiles was significantly affected by K_m but not by V_{max}.

Figure 7 shows the relationship between the hepatic up-

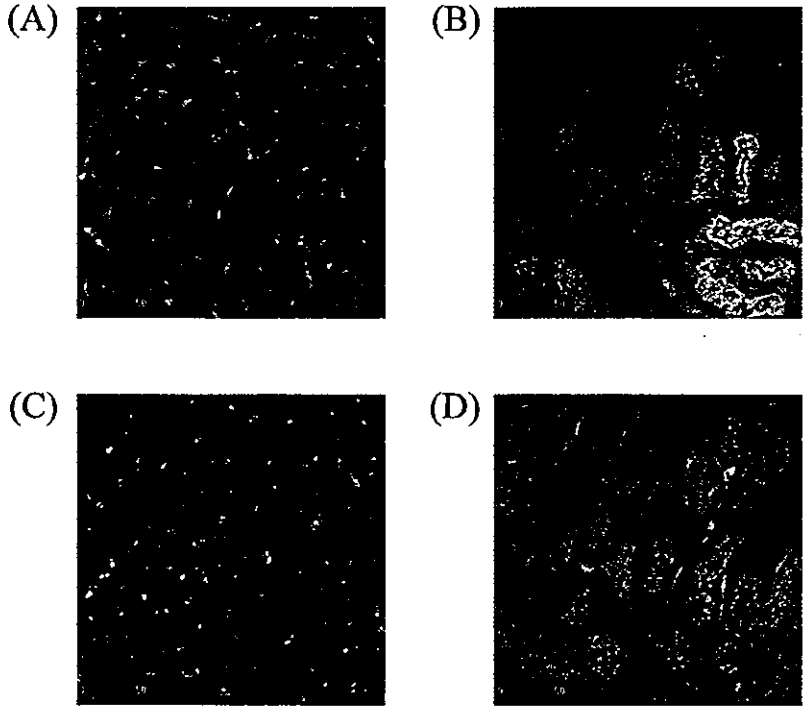

Fig. 3. Confocal microscopic images of liver (A and C) and kidney (B and D) sections of mice 10 min after intravenous injection of FITC-labeled Suc_{54}-BSA at a dose of 20 mg/kg. Green signals are derived from FITC-Suc_{54}-BSA and red ones from PI for nuclear staining (A and B) or from rhodamine for vascular endothelial cells (C and D). Yellow color indicates that FITC and rhodamine colocalize in the same site.

take clearances and the injected dose of Suc-IgGs (Fig. 7A) and Suc-BSAs (Fig. 7B) based on the experimental data. The hepatic uptake clearance values decreased, and the slope of the dose-hepatic uptake clearance curve decreased, in parallel with the reduction in the number of succinylated amino groups. Together with the results of the computer simulation study (Fig. 6), these results suggest that the affinity for SRs in the liver depends on the surface density of the succinylated amino groups on Suc-IgGs and Suc-BSAs. Moreover, the slope of Suc_{20}-BSA was almost equal to that of Suc_{50}-IgG, whose surface density of succinylated amino groups was similar to that of Suc_{20}-BSA. These results show that molecular size and the surface density of succinylated amino groups were important for recognition of hepatic SRs.

Pharmacokinetic Analysis of Distribution Profiles of Succinylated Proteins Based on a Physiological Model. Differential eqs. 1 to 3 were simultaneously fitted to the experimental data of the plasma concentrations and liver accumulation of each ^{111}In-Suc-BSA, and four parameters ($K_{m,l}$, $V_{max,l}$, $K_{m,p}$, and $V_{max,p}$) were estimated (Table 3). The estimated parameters properly describe the distribution profiles of Suc-BSAs (data not shown). Figure 8 illustrates the $K_{m,l}$ and $K_{m,p}$ values of all Suc-BSAs plotted against the surface density of the succinylated amino groups. These parameters, $K_{m,l}$ and $K_{m,p}$, which correspond to the affinity of the succinylated proteins for hepatic uptake and extrahepatic elimination, respectively, correlated with the surface density of the succinylated amino groups (Fig. 8). With an increase in the surface density, $K_{m,l}$ decreased from 2500 nM for Suc_{20}-BSA to 5.3 nM for the Suc_{54}-BSA, and $K_{m,p}$ decreased from 24,000 nM to 230 nM. On the other hand, $V_{max,l}$ and $V_{max,p}$ remained relatively constant. The parameters of Suc_{50}-IgG were also plotted to examine the correlation for Suc-BSAs. These results suggested that the in vivo affinity of the succinylated proteins for SRs was closely related to the surface density of the succinylated amino groups on the modified proteins.

Discussion

In recent years, several new members of the SR family have been cloned on the basis of their ability to recognize

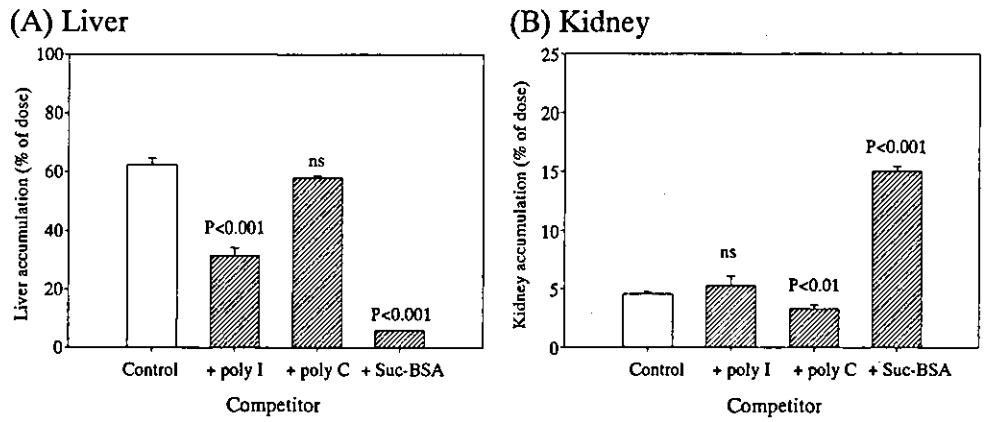

Fig. 4. Competition of hepatic and renal uptake of ^{111}In-Suc_{54}-BSA by preadministration of poly I, poly C, or Suc_{54}-BSA after intravenous injection in mice. [^{111}In]Suc_{54}-BSA (0.1 mg/kg) was injected 1 min after injection of unlabeled competitive macromolecules (20 mg/kg). Results were expressed as mean ± S. D. of three mice. Statistically significant difference based on Student's t test compared with each control.

TABLE 2
AUC and clearances of ^{111}In-labeled succinylated proteins in mice after intravenous injection at the doses of 0.1, 1, 10, and 20 mg/kg
AUC and clearances were calculated from experimental data shown in Fig. 2.

Compound	Dose	AUC	Clearance			
			CL_{total}	CL_{liver}	CL_{kidney}	CL_{urine}
	mg/kg	*hr · % of dose/ml*			*ml/hr*	
SOD	0.1	6.83	14.6	0.04	13.0	0.18
	20	6.97	14.3	0.03	5.20	3.56
Suc_9-SOD	0.1	5.73	17.5	0.05	13.6	0.74
	1	4.88	20.5	0.06	13.5	2.59
	10	5.84	17.1	0.04	4.45	5.30
	20	4.75	21.0	0.04	4.73	8.93
Suc_{22}-SOD	0.1	4.61	21.7	1.04	2.98	4.10
	1	3.48	28.7	1.19	2.51	7.33
	10	3.42	29.2	1.06	3.49	5.56
	20	4.34	23.1	0.08	2.86	7.37
BSA	0.1	145.96	0.69	0.002	0.020	0.002
	20	144.97	0.69	0.013	0.024	0.002
Suc_{20}-BSA	0.1	144.93	0.69	0.42	0.03	0.006
	1	201.61	0.50	0.29	0.04	0.005
	10	85.69	1.17	0.20	0.08	0.02
	20	134.95	0.74	0.20	0.06	0.01
Suc_{28}-BSA	0.1	6.46	15.5	9.35	1.23	0.39
	1	16.21	6.17	3.67	0.14	0.02
	10	44.74	2.24	0.81	0.23	0.11
	20	65.66	1.52	0.66	0.17	0
Suc_{40}-BSA	0.1	1.54	64.9	48.0	1.82	0.17
	1	4.34	23.0	14.4	0.94	0.26
	10	22.03	4.54	2.22	0.49	0.03
	20	27.83	3.59	1.46	0.60	0.04
Suc_{46}-BSA	0.1	0.71	140.5	72.2	3.46	1.14
	1	4.31	23.2	12.5	1.07	1.69
	10	23.70	4.22	1.37	0.93	0.54
	20	20.44	4.89	1.53	1.04	0.24
Suc_{54}-BSA	0.1	0.71	141.5	69.4	5.59	2.31
	1	2.95	33.9	14.7	2.63	1.31
	10	22.20	5.40	0.81	1.20	0.29
	20	23.29	4.29	0.35	1.42	0.25
IgG	0.1	138.52	0.72	0.03	0.02	0.056
	20	250.01	0.40	0.02	0.01	0.046
Suc_{22}-IgG	0.1	164.58	0.61	0.04	0.02	0.006
	1	237.12	0.42	0.03	0.02	0.005
	10	213.69	0.46	0.04	0.02	0.003
	20	215.84	0.46	0.04	0.02	0.02
Suc_{50}-IgG	0.1	6.16	16.2	7.39	0.64	0.50
	1	18.76	5.33	2.44	0.22	0.10
	10	47.35	2.11	0.84	0.10	0.04
	20	34.91	2.86	0.07	0.07	0.02

modified lipoproteins, and the family has been divided into six classes (Terpstra et al., 2000). The distinct, but partly overlapping, binding properties of the SR classes represent a complication in defining their respective activity in terms of ligand uptake. Most SRs can bind a variety of polyanionic ligands, including negatively charged albumins. Since many of the SRs are expressed in sinusoidal endothelial cells and Kupffer cells in the liver, plural SRs may be responsible for the hepatic uptake of succinylated proteins. We and others have shown that highly succinylated albumins are extensively taken up by mouse and rat liver (Franssen et al., 1993; Jansen et al., 1993; Takakura et al., 1994; Furitsu et al., 1997; Kuipers et al., 1997). Although both Kupffer cells and liver endothelial cells were involved in the uptake, the endothelial cells made the greatest contribution. The hepatic uptake of Suc-BSA was significantly inhibited by maleylated BSA, dextran sulfate, and poly I but not by poly C. This inhibition profile was similar to that observed in class AI/AII SRs (SRA), the most well characterized SRs (Krieger, 1992; Gough and Gordon, 2000). For a rational design of succinylated proteins for SR-mediated targeting, it is necessary to understand the quantitative relationship between the physicochemical characteristics and the nonlinear in vivo pharmacokinetics. Although our previous studies suggested the importance of the molecular weight of proteins (Takakura et al., 1994; Furitsu et al., 1997), a detailed analysis of this

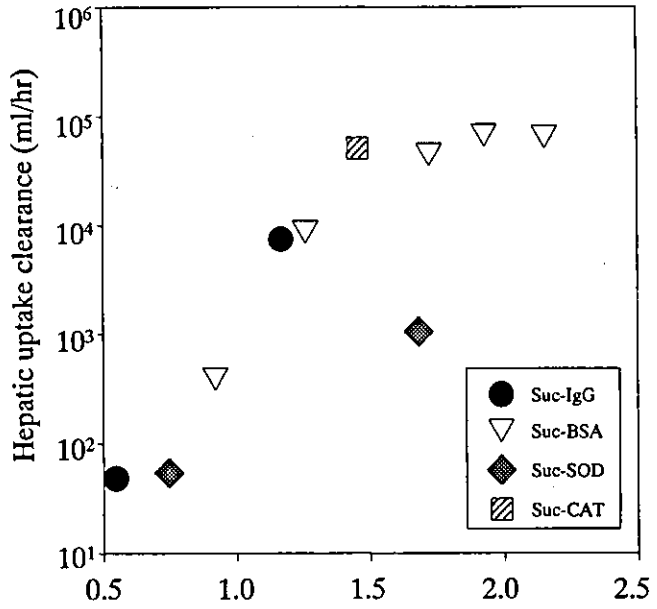

Fig. 5. Estimated surface density of succinylated amino groups × 10^3 (molecules/Å^2). Hepatic (A) and renal (B) uptake clearances of ^{111}In-labeled Suc-IgG (●), Suc-BSA (▽), Suc-SOD (◆), and succinylated catalase (▨) in mice after intravenous injection at a dose of 0.1 mg/kg.

remained to be carried out. In the present study, a systematic pharmacokinetic study was performed using a series of succinylated proteins with various molecular weights and degree of modification to achieve this aim.

In this study, we used ^{111}In-labeled succinylated proteins that are more suitable than those labeled with radioiodine to estimate the tissue distribution since the radioactivity remains within the lysosomes and is only slowly released from cells after receptor-mediated endocytosis. This property enables us to quantitatively determine the tissue distribution by counting radioactivity. However, the amount of ^{111}In radioactivity in tissues gradually decreased in some cases, especially the hepatic accumulation of highly succinylated proteins at lower doses (Fig. 2). Therefore, we used the distribution data showing no obvious decrease in radioactivity to calculate the organ uptake clearances and to fit the differential equations to the experimental data.

The present study has demonstrated that succinylated proteins are selectively taken up by liver nonparenchymal cells via SRs according to the degree of succinylation and the injected dose. Confocal microscopic studies, including immunohistochemical studies, showed a significant contribution of the liver nonparenchymal cells, especially endothelial cells, to the hepatic uptake of Suc-BSA (Fig. 3). Furthermore, involvement of the SR was confirmed by the competition experiments using poly I, a typical ligand for the receptor (Fig. 4). The hepatic uptake clearance correlated well with the estimated surface density of the succinylated amino groups, suggesting that a negative charge density is a critical factor for recognition by SRs. Further pharmacokinetic analysis showed that the affinity corresponded well to the negative charge density. Suc_{22}-SOD, however, failed to be taken up by the liver regardless of its high negative-charge density. Taken together, these results suggest that not only the negative-charge density, but also the molecular weight or size is important. These findings provide useful guidelines for the development of targeted delivery systems using succinylated proteins. To design a molecule for efficient SR-mediated hepatic targeting, a protein larger than BSA, having a succinylated amino group density of about 1.5 × 10^3 molecules/Å^2, should be used. Higher densities than this will not dramatically increase targeting efficacy. This information will be important when succinylation is applied to biologically active proteins, such as enzymes. Since unnecessary chemical modification sometimes impairs the activity, an appropriate min-

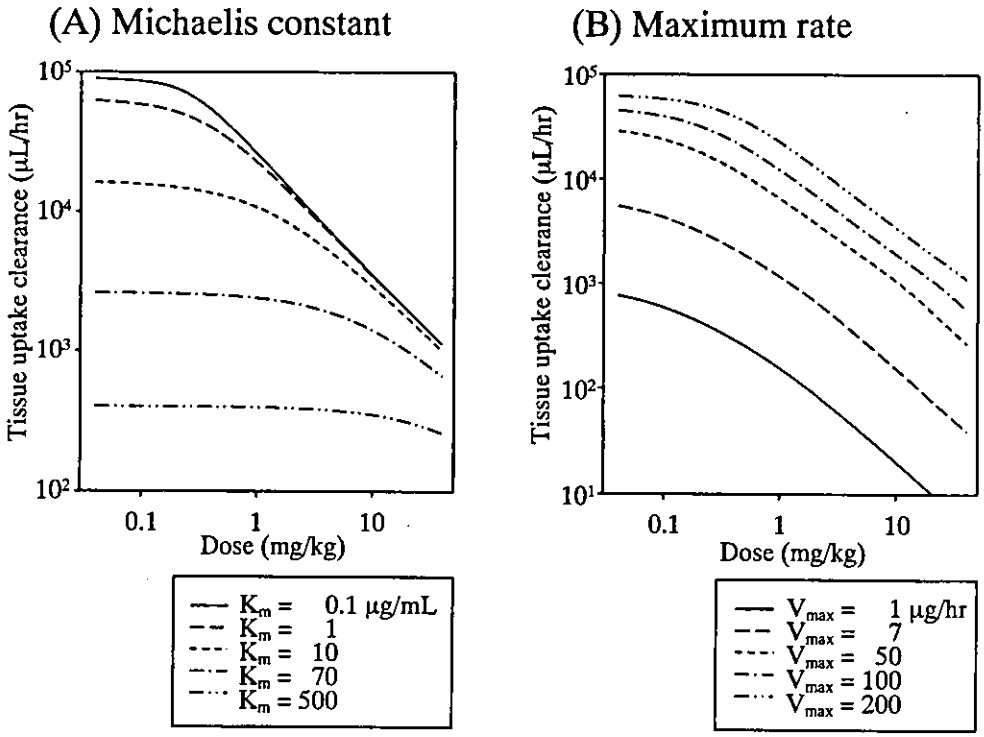

Fig. 6. Simulation of the effect of pharmacokinetic parameters [i.e., Michaelis constant (A) and maximum rate (B)] on the relationship between the tissue uptake clearance and injected dose.